



University of Potsdam
Institute of Geosciences

Master's thesis

Measuring high-resolution surface deformation signals in Turkey using Sentinel-1 radar interferometry

by
Yiğit Öner Altıntaş

Supervisors

Dr. Jonathan R. Weiss
Prof. Dr. Bodo Bookhagen

Potsdam, 24.02.2022

Declaration of Authorship

I, Yiğit Öner Altıntaş, hereby declare that this thesis is the product of my own work. All the assistance received in preparing this thesis and the sources used have been acknowledged.

Signature:

Date: 24.02.2022

Eidesstattliche Erklärung

Hiermit erkläre, Yiğit Öner Altıntaş, dass diese Arbeit das Ergebnis meiner eigenen Arbeit ist. Alle bei der Erstellung dieser Arbeit erhaltenen Hilfestellungen und die verwendeten Quellen wurden gewürdigt.

Unterschrift:

Datum: 24.02.2022

Abstract

Episodic fault creep (i.e., slow, aseismic slip) is an important component of tectonic deformation. The detection of creep events has been greatly facilitated by geodetic measurements, including the role these events play in the seismic cycle. Creep can release as much energy as an earthquake and has been identified in a number of faults around the globe. One such location is the North Anatolian Fault (NAF) in Turkey. Several portions of the NAF exhibit slow-slip behavior as post-seismic slip (after an earthquake). In addition, one portion of the NAF shows a “slip-burst” pattern, meaning that a year’s worth of slip occurs in a short period of time (~1 month). Here I investigate slip-burst behavior across the Ismetpasa segment of the NAF using ~6 years of high temporal and high spatial resolution Sentinel-1 interferometric synthetic aperture radar (InSAR) data. I identify at least 3 slip-bursts that occurred in June 2016, 2017, and 2018. The duration of each burst was ~1 month. The line-of-sight (LOS) slip rate associated with these bursts is ~6 mm/yr, which satisfies yearly creep slip deficit on this segment. The effect of the bursts extends ~2250 m away from the fault. In addition to the slip burst analysis, I derived a new, high-resolution strain field for Anatolia that clearly reveals creeping portions of the NAF and potentially some previously unrecognized active faults. This study confirms that episodic creep events can be clearly identified and analyzed using Sentinel-1’s high-resolution (temporal + spatial) interferometry data. Additional noise suppression and/or longer InSAR time series will enhance future efforts aimed at achieving a more detailed understanding of Anatolian active tectonics.

Zusammenfassung

Episodisches Verwerfungskriechen (d. h. langsames, aseismisches Gleiten) ist eine wichtige Komponente der tektonischen Verformung. Die Erkennung von Kriechereignissen wurde durch geodätische Messungen erheblich erleichtert, einschließlich der Rolle, die diese Ereignisse im seismischen Zyklus spielen. Kriechen kann so viel Energie freisetzen wie ein Erdbeben und wurde in einer Reihe von Verwerfungen auf der ganzen Welt festgestellt. Ein solcher Ort ist die Nordanatolische Verwerfung (NAF) in der Türkei. Mehrere Teile des NAF zeigen ein Slow-Slip-Verhalten als postseismischer Schlupf (nach einem Erdbeben). Darüber hinaus zeigt ein Teil des NAF ein „Slip-Burst“-Muster, was bedeutet, dass ein Jahresrutsch in kurzer Zeit (~1 Monat) auftritt. Hier untersuche ich das Slip-Burst-Verhalten im gesamten Ismetpasa-Segment der NAF unter Verwendung von Sentinel-1-Daten mit hoher zeitlicher und räumlicher Auflösung von Sentinel-1 mit interferometrischer synthetischer Apertur (InSAR). Ich identifiziere mindestens 3 Slip-Bursts, die im Juni 2016, 2017 und 2018 auftraten. Die Dauer jedes Bursts betrug ~1 Monat. Die mit diesen Ausbrüchen verbundene Sichtlinienschlupfrate (LOS) beträgt ~6 mm/Jahr, was das jährliche Kriechschlupfdefizit in diesem Segment befriedigt. Die Wirkung der Bursts erstreckt sich ~2250 m von der Verwerfung entfernt. Zusätzlich zur Slip-Burst-Analyse leitete ich ein neues, hochauflösendes Dehnungsfeld für Anatolien ab, das deutlich kriechende Teile der NAF und möglicherweise einige zuvor nicht erkannte aktive Verwerfungen aufzeigt. Diese Studie bestätigt, dass episodische Kriechereignisse mithilfe der hochauflösenden (zeitlichen + räumlichen) Interferometriedaten von Sentinel-1 eindeutig identifiziert und analysiert werden können. Zusätzliche Rauschunterdrückung und/oder längere InSAR-Zeitreihen werden zukünftige Bemühungen verstärken, die darauf abzielen, ein detaillierteres Verständnis der aktiven Tektonik Anatoliens zu erreichen.

Acknowledgements

I was fortunate to interact amazing people until this point in my life. A few of them are mentioned below.

I'd like to thank my main supervisor Dr. Jonathan R. Weiss for his support since I sent an email to him when I was just beginning my studies at Uni-Potsdam. He always created a time window for me even in these difficult pandemic times in last two years (even when there is a staggering 12 hours between our time zones!).

I'd like to thank Prof. Bodo Bookhagen not just for his amazing feedback or his wisdom but also for his tireless efforts for organizing number of things, including maintaining a master's program!

I'm so lucky to have Dr. Christopher Kyba from GFZ-Potsdam as my mentor. He taught me how to become a great scientist and a great person overall, thank you Chris, so many things wouldn't be possible if it wasn't for you, including this thesis.

I'd like to thank my parents, they always trusted me, no matter how crazy I sound some time.

And lastly, I'd like to thank my fiancée, İdil, for pushing me in my studies and transferring her luck to me ☺.

Contents

DECLARATION OF AUTHORSHIP	II
ABSTRACT.....	III
ACKNOWLEDGEMENTS	V
LIST OF FIGURES	VII
1. INTRODUCTION	1
2. STUDY AREA.....	5
2.1. NORTH ANATOLIAN FAULT.....	6
2.2. ISMETPASA SEGMENT	7
3. DATA AND METHODS	9
3.1. STRAIN MAPPING.....	9
3.2. SAR INTERFEROMETRY.....	9
3.3. SENTINEL-1	11
3.4. LiCSAR	11
3.5. LiCSBAS.....	12
3.6. GACOS ATMOSPHERIC CORRECTION SERVICE	14
3.7. TIME SERIES ANALYSIS	15
4. RESULTS	16
4.1. HIGH-RESOLUTION STRAIN MAP FOR ANATOLIA	17
4.2. PROFILES ON NAF.....	17
4.3. 3D DEFORMATION TIME-SERIES FOR THE NAF	20
4.4. TEMPORAL EVOLUTION OF A SWATH IN TIME-SERIES.....	23
5. DISCUSSION.....	26
5.1. CREEPING AREAS DERIVED FROM STRAIN MAP	26
5.2. LOCKED VS CREEPING SECTION OF THE NAF.....	28
5.3. ACROSS-TRACK CREEP INFLUENCE EXTENT	30
5.4. EPISODIC SLIP-BURST ON NAF	32
6. CONCLUSION.....	35
A. APPENDIX.....	36
A.1. NOISY DATE PAIRS FROM ALL 3 PROFILES.....	36
A.2. AUTOMATION OF DATE PAIR CREATION.....	37
A.3. USED DATES	38
BIBLIOGRAPHY	39

List of Figures

FIGURE 1.1: A VERY BROAD VIEW OF SEISMIC CYCLE ON A STRIKE-SLIP FAULT.....	1
FIGURE 1.2: THEMATIC VIEW OF STRAIN ACCUMULATION ON STRIKE-SLIP FAULTS (NOT-TO-SCALE). STRAIN RELEASE WITH A VISIBLE OFFSET ON TOPOGRAPHY GENERALLY IS A RESULT OF RELATIVELY BIG EARTHQUAKE ($>M\sim 6.0$). FIGURE REDRAWN FROM [20] HUSSAIN, 2016.....	2
FIGURE 1.3: BASICS OF SENTINEL-1 RADAR INTERFEROMETRY IN GEODETIC TECTONICS. FIGURE SIMPLIFIED AND REDRAWN FROM [30] OSMANOGLU ET AL., 2016.	3
FIGURE 1.4: SLIP-BURST SIGNAL ON ISMETPASA SEGMENT OF THE NORTH ANATOLIAN FAULT, MEASURED WITH COSMO-SKYMED CONSTELLATION DATA. FIGURE FROM [34] ROUSSET ET AL., 2016.....	4
FIGURE 2.1: TECTONIC SETTING OF ANATOLIA AND SURROUNDINGS. NUMBERS SHOW GNSS DERIVED MOVEMENT IN MM/YR RELATIVE TO STABLE EURASIA. NUMBERS IN PARENTHESIS SHOW STRIKE-SLIP FAULT RATES. EAF IS EAST ANATOLIAN FAULT. SLIP RATES AND BOUNDARIES FROM [33] REILINGER ET AL., 2006.	5
FIGURE 2.2: EARTHQUAKE PROPAGATION ON THE NORTH ANATOLIAN FAULT. NOTICE EARTHQUAKE EVENTS STARTING WITH 1939 M7.9, MAINLY TRANSFERS STRESS TO NEXT WESTERN SEGMENT. FIGURE FROM [20] HUSSAIN, 2016.	6
FIGURE 2.3: MAIN CREEPING SEGMENTS OF THE NORTH ANATOLIAN FAULT (NAF) SHOWN WITH YELLOW DASHED LINES. RED RECTANGLE SHOWS THE STUDY AREA OF THIS THESIS. FAULTS FROM [17] EMRE ET AL., 2018.....	7
FIGURE 2.4: STUDY AREA OF THIS THESIS SHOWN WITH RED RECTANGLE. ISMETPASA SEGMENT HAS BEEN INDICATED WITH YELLOW DASHED LINE. FAULTS FROM [17] EMRE ET AL., 2018.	8
FIGURE 3.1: AN EXAMPLE INTERFEROGRAM SHOWING THE DEFORMATION OF 2003 M6.6 IRAN-BAM EARTHQUAKE. FRINGES INDICATE THE PHASE DIFFERENCE BETWEEN THE IMAGES TAKEN BEFORE AND AFTER EARTHQUAKE. PHOTO FROM ESA WEBSITE [40].....	10
FIGURE 3.2: STUDY AREA CLIPPED FROM LICSAR ASCENDING FRAME WITH THE ID 087A_04904_121313. THE FAULT WITH THE ARROWS IS THE NORTH ANATOLIAN FAULT. FAULTS FROM EMRE ET AL., 2018.	12
FIGURE 3.3: TWO MAIN PARTS OF LICSBAS WORKFLOW CAN BE SEEN ON LEFT AND RIGHT SIDES. FIGURE FROM [29] MORISHITA ET AL., 2020.	13
FIGURE 3.4: PERPENDICULAR BASELINE FOR THE STUDY AREA, MEANING RELATIVE SPATIAL POSITION OF THE SENTINEL-1 SENSORS IN SPACE/TIME FOR EACH IMAGE. NOTICE HOW SENTINEL-1B LAUNCH IN APRIL 2016 MADE TEMPORAL RESOLUTION INCREASE SIGNIFICANTLY.	14
FIGURE 3.5: IMPACT OF GACOS CORRECTION. THE LEFT PANEL SHOWS BEFORE AND AFTER STANDARD DEVIATION DISTRIBUTION OF INTERFEROGRAMS. RIGHT PANEL SHOWS REDUCTION RATE FOR EACH INTERFEROGRAM.	15
FIGURE 4.1: EVOLUTION OF TECTONIC DEFORMATION IN THE STUDY AREA. STARTING WITH PANEL (E), TOPOGRAPHIC SIGNAL CAN BE SEEN WHICH ASSUMED TO BE ERROR AND FURTHER DISREGARDED IN FOLLOWING ANALYSIS. A	

LINEAR DEFORMATION ASSUMED TO BE TECTONIC SIGNAL CAN BE SEEN ALONG THE NORTH ANATOLIAN FAULT.	
BLUE RECTANGLE SHOWS THE STABLE REFERENCE AREA.....	16
FIGURE 4.2: COMPARISONS BETWEEN [39] WEISS ET AL., 2020 AND THIS STUDY'S HIGH-RESOLUTION STRAIN RATES.	
SHARPER STRAIN RATES CAN BE SEEN ON THE LEFT PANELS. 10^{-9} YR $^{-1}$ IS NANO-STRAIN.....	17
FIGURE 4.3: THREE 8 KM * 1 KM PROFILES USED IN THIS STUDY. PROFILE (A) IS ON LOCKED PORTION, PROFILE (B)	
AND (C) ARE ON THE CREEPING PORTION ON THE NORTH ANATOLIAN FAULT. THE BLUE RECTANGLE SHOWS THE	
REFERENCE AREA FOR THE RASTER. FAULTS FROM EMRE ET AL., 2018.....	18
FIGURE 4.4: ELEVATION OF PROFILES (A), (B) AND (C) ON THE NORTH ANATOLIAN FAULT.....	18
FIGURE 4.5: A SCHEMATIC VIEW OF AUTOMATED WAY OF CREATION OF INDIVIDUAL CUMULATIVE DISPLACEMENT	
FILES AND AN EXAMPLE PROFILE SIZE.....	19
FIGURE 4.6: AN EXAMPLE OF CUMULATIVE DISPLACEMENT SCATTER POINTS FOR ONE DATE PAIR FOR PROFILE (B).	
THERE ARE 707 SCATTERS OUT OF 882 (NORMALLY) IN THIS PLOT. THE REST ARE MASKED FOR THIS INDIVIDUAL	
DATE PAIR.....	20
FIGURE 4.7: SCATTERS OF 255 INTERFEROGRAMS STARTING IN 2014. EVOLUTION OF THE PROFILE (B) BETWEEN	
10.11.2014 AND 06.23.2020. NAF IS AT KM "0". REFERENCE DATE FOR ALL DATE PAIRS IS OCTOBER 14 TH ,	
2014.....	21
FIGURE 4.8: EVOLUTION OF CREEPING PROFILE (B) IN ~6 YEARS WITH RED LINES SHOWING THE AVERAGE POSITIONS	
OF SCATTERS.....	22
FIGURE 4.9: PROFILE (A) TEMPORAL EVOLUTION FOR ~6 YEARS. THIS IS A "LOCKED PORTION" OF THE NAF.....	22
FIGURE 4.10: TEMPORAL LOS DEFORMATION EVOLUTION OF CREEPING PROFILE (C) IN ~6 YEARS. THIS IS A CREEPING	
SECTION OF THE FAULT, LIKE PROFILE (B).....	23
FIGURE 4.11: TIME SERIES FOR LOS DEFORMATION FOR PROFILE (B). BLUE AND ORANGE LINES ARE SHOWING THE	
MEAN VALUE OF A SWATH CENTERED AT ~300 METERS. BLUE AND ORANGE LINES ARE ~500 M APART FROM	
EACH OTHER. GREEN LINE IS THE DIFFERENCE BETWEEN BLUE AND ORANGE LINES.....	24
FIGURE 4.12: TEMPORAL EVOLUTION OF PROFILE (B), WITH THE ERROR ENVELOPES. BLUE LINE IS TAKEN FROM A	
SWATH FROM SOUTHERN PART OF FAULT. ORANGE LINE IS FROM NORTHERN PART. GREEN LINE IS THE	
DIFFERENCE BETWEEN ORANGE AND BLUE LINES. ERROR ENVELOPE AROUND THE GREEN LINE IS THE RESULT OF	
SIMPLE ERROR PROPAGATION.....	25
FIGURE 5.1: HIGH RESOLUTION STRAIN MAP FOR ANATOLIA. A, B, C AND D SHOWS CERTAIN PARTS OF NAF. RED	
RECTANGLE IN PANEL C SHOWS THE FOCUS OF THIS THESIS. FAULTS FROM [17] EMRE ET AL., 2018.....	26
FIGURE 5.2: STRAIN PROFILES ON THE ISMETPASA CREEPING SEGMENT ON NORTHERN ANATOLIAN FAULT.....	27
FIGURE 5.3: TWO OTHER AREAS THAT IS SHOWING 1000+ NST/YEAR. SOURCE OF DEFORMATION ON LEFT FIGURE	
COULD BE 2020 Mw 6.8 ELAZIG EARTHQUAKE. HIGH-STRAIN FIELD ON THE RIGHT IS ON BERENDI FAULT BUT	
NOT CORRELATED WITH THE FAULT. FAULTS FROM [17] EMRE ET AL., 2018.....	28
FIGURE 5.4: PROFILE (A) "LOCKED" AND (C) "CREEPING" EVOLUTION IN ~6 YEARS WITH TEMPORAL CHANGE. GREEN	
LINE AND MAGENTA LINE ARE SHOWING THE DIFFERENCE BETWEEN THEIR CORRESPONDING BLUE AND ORANGE	
SWATHS.....	29

FIGURE 5.5: COMPARISON OF DIFFERENCES BETWEEN CREEPING AND LOCKED SECTIONS. CREEPING SECTION IS PROFILE (C), LOCKED SECTION IS PROFILE (A).....	30
FIGURE 5.6: SWATH PAIRS LOCATED AT ~500, ~1500 AND ~3000 M EITHER SIDE FROM THE FAULT. GREEN LINE SHOWS THE DIFFERENCE BETWEEN SWATHS TAKEN FROM 500 M APART FROM THE FAULT (~1000 M APART FROM EACH OTHER). BROWN SHOWS ~1500 M AND PURPLE SHOWS ~3000 M.....	31
FIGURE 5.7: TEMPORAL EVOLUTION OF DIFFERENCES OF SWATH PAIRS TAKEN FROM EVERY 500 M STEP DISTANCES FROM EITHER SIDE OF NORTH ANATOLIAN FAULT.	32
FIGURE 5.8: LINEAR FIT IN-BETWEEN EVERY 3 MONTHS FOR THE SWATH PAIR WITH ~250 M DISTANCE FROM THE FAULT FOR PROFILE (B). 5 CANDIDATES FOR SLIP-BURSTS SHOWN IN THE TOP SIDE.....	33
FIGURE 5.9: HORIZONTAL FIT FOR THE TIME-SERIES, SEPARATED WITH MOST ABRUPT SIGNAL CHANGES. RED PANEL BEHIND THE LINES SHOW THE DURATION OF EVENTS.	34
FIGURE A.1: A SIDE VIEW OF 3D SCATTER TIME-SERIES. CHANGED DATA PAIRS FROM PROFILES ARE SHOWN WITH RED SCATTERS.	36

1. Introduction

An earthquake is a release of accumulated stress in a period on an underlying fault. They sometimes can be so hazardous that they could cause so many human lives, such as 1999 Izmit Earthquake in Turkey ([4] Barka, 1999). However, stress on faults sometimes released in a “slow” manner (~years to ~decades) in contrast to earthquakes and these slow slip events can release stress as much as of an earthquake ([22] Jolivet et al., 2020). States of an earthquake cycle generally could be explained with a broad view of seismic cycle (Figure 1.1).

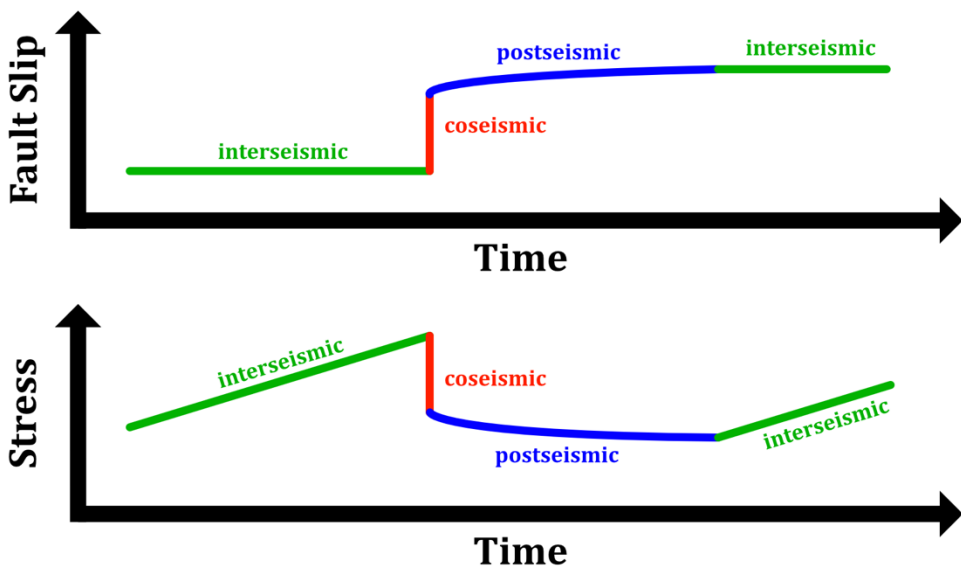


Figure 1.1: A very broad view of seismic cycle on a strike-slip fault.

Accordingly, in the interseismic period the fault accumulates stress (varies from ~centuries to ~decades) without any slow slip. A coseismic period is where the actual earthquake happens (varies from ~seconds to ~minutes) (Figure 1.2). In a postseismic state, fault slips slowly with number of earthquakes very small in magnitude (mostly < M2.0). Postseismic state can be a slow slip with stress accumulation (rare event) therefore postpones the coseismic (earthquake) event. Postseismic state can also be a slow slip with stress release. All in all, understanding the underlying mechanisms of the seismic cycle of an earthquake series is crucial for seismic hazard assessment.

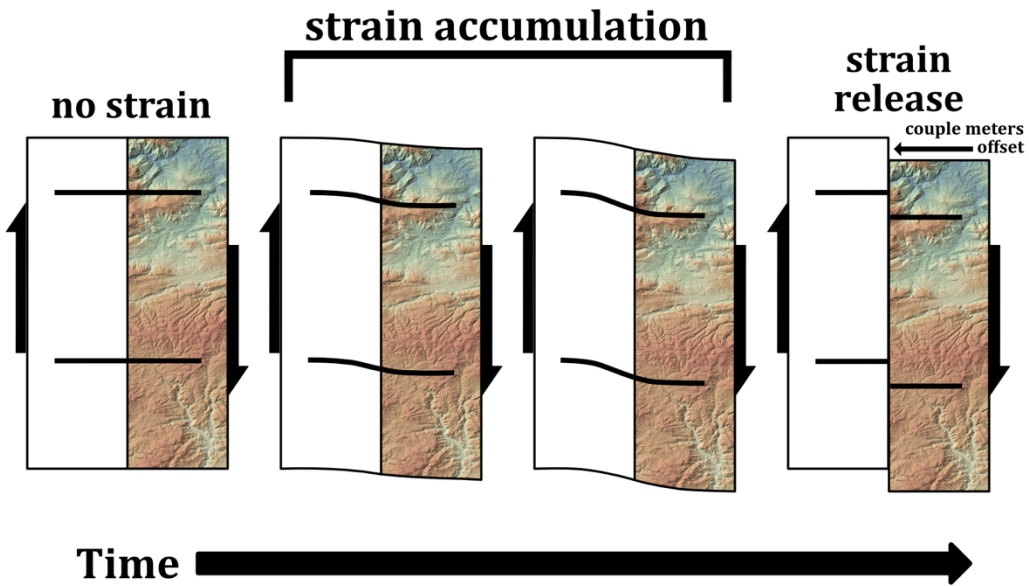


Figure 1.2: Thematic view of strain accumulation on strike-slip faults (not-to-scale). Strain release with a visible offset on topography generally is a result of relatively big earthquake ($>M \sim 6.0$). Figure redrawn from [20] Hussain, 2016.

Understanding fault mechanisms starts with detecting earth surface movements, which should be done relative to a stable part of the surface. The source of surface movements can be volcanic, anthropogenic, or tectonic. The sparse GNSS network (Global Navigation Satellite System) and InSAR (Interferometric Synthetic Aperture Radar) derived measurements can be two good candidates for the job. They both individually have pros and cons, for example GNSS-derived data is more stable in signal quality but lacks in spatial extent. The InSAR method on the other hand, has a bigger spatial extend but mostly limited by its signal-to-noise ratio. But after several corrections and noise removal, InSAR measurements can be a game changer in geodetic tectonic measurements. The different types of deformation signals like volcanic ([19] Hooper et al., 2004), anthropogenic ([38] Tung et al., 2012), glacier movement tracking ([28] Mohr et al., 1998) and tectonic are detectable with InSAR measurements. But InSAR doesn't only contain deformation signal. It also contains signals interacted with topography, atmosphere, temporal decorrelation, noise etc. To get the valuable deformation signal, unwanted signals should be removed, for this reason there are several software which are able to remove noise as much as possible. I've used LiCSBAS for this study, to remove the noise and for the time-series extraction, more info on these will be given in InSAR section of this study. A simplified InSAR schematic can be seen in Figure 1.3.

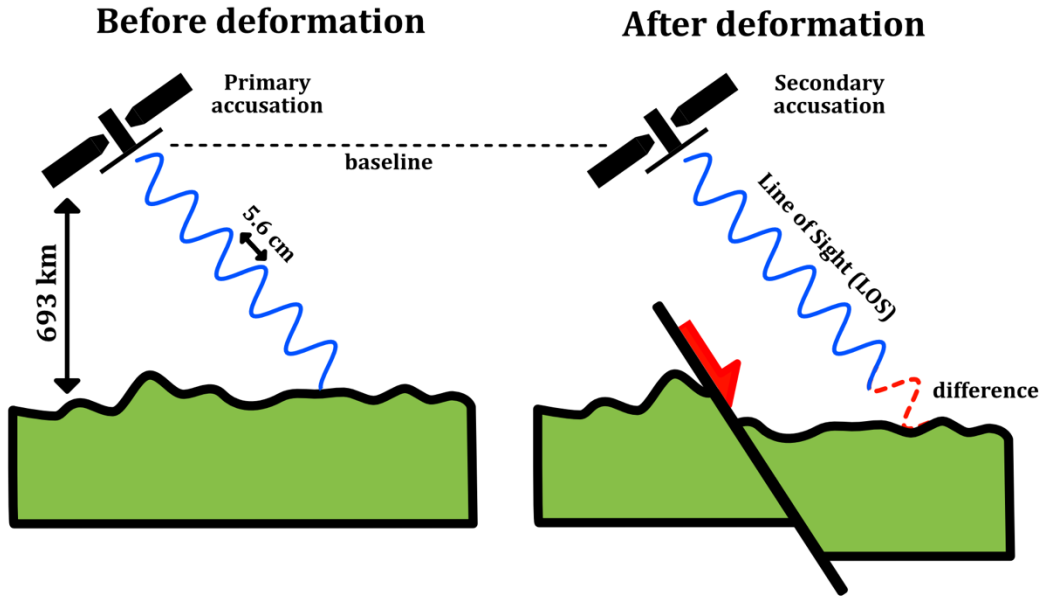


Figure 1.3: Basics of Sentinel-1 radar interferometry in geodetic tectonics. Figure simplified and redrawn from [30] Osmanoglu et al., 2016.

North Anatolian Fault (NAF) in Turkey is a ~ 1200 km major tectonic feature, acting as a boundary between Anatolian Plate and Eurasian Plate ([8] Bozkurt, 2001). There have been several West propagating earthquakes in the last 100 years on the fault resulted in a huge number of human lives. The slip rate of the whole Anatolian Plate is ~ 20 mm/yr and the slip rate on the NAF is ~ 25 mm/yr ([33] Rousset et al., 2016). Creeping sections (or also called slow slip events (SSE)) on the NAF are generally known, published for different portions. For example, creeping of Izmit-Akyazi segment has been shown by [11] Cakir et al., 2012 and creeping of Marmara segment has been shown by [7] Bohnhoff et al., 2017, [42] Yamamoto et al., 2019. Ismetpasa segment is one of those creeping segments and it also has been shown by [34] Rousset et al., 2016, that a slip-burst event happened recently back in 2014 (Figure 1.4). They characterized single slip-burst event by a relatively fast-slip (\sim a month in temporal scale and around ~ 15 mm in spatial scale) without an earthquake. Episodic slip-burst however can be best shown with a line-of-sight (LOS) time series of surface deformation ([22] Jolivet et al., 2020). I'll elaborate more on North Anatolian Fault and its creeping sections in next section of my thesis.

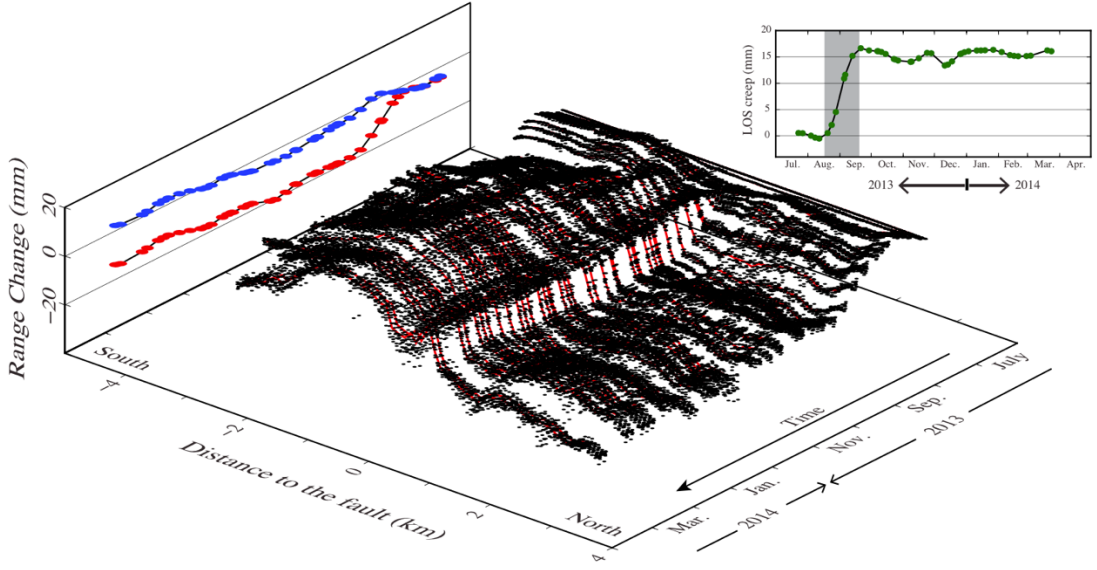


Figure 1.4: Slip-burst signal on Işmetpasa Segment of the North Anatolian Fault, measured with COSMO-SkyMed constellation data. Figure from [34] Rousset et al., 2016.

In this study I've produced high temporal and high spatial resolution InSAR time series to measure surface deformation on a specific creeping segment on the North Anatolian Fault. I've done the analysis on the same profile parameters as [34] Rousset et al., 2016 (Figure 1.4). However, in contrast to [34] Rousset et al., 2016 have been used, which is 10 months of COSMO-SkyMED data, I've used \sim 6 years of Sentinel-1 data. I also have used a different time-series analysis package and interferogram production platform (LiCSBAS and LiCSAR). In addition, I've also produced high-resolution strain map by using InSAR derived and GNSS derived filtered velocity fields for whole Anatolia which has a potential to show creeping areas. I've also compared the high-resolution strain rate map with what [39] Weiss et al., 2020 has been done. These measurements have the potential to help better understand underlying mechanisms on strike-slip faults with creeping behavior.

2. Study Area

Anatolia, being amid three massive tectonic plates (African, Eurasian and Arabia) shows great amount of surface deformation (Figure 2.1). With the Arabian Plate moving Northward, Anatolian micro-Plate gets squeezed against the stable Eurasian Plate. Therefore, Anatolian Plate gets pushed to Westward, into the Hellenic Subduction Zone. These movements, result with so called tectonic-escape deformation ([8] Bozkurt, 2001), which creates multiple tectonic features in the region. These are North Anatolian Fault (NAF) which is corresponding to boundary between Eurasian Plate and Anatolian Plate, East Anatolian Fault (EAF) which is the boundary between Anatolian Plate and Arabian Plate and lastly the Hellenic Subduction Zone. These natural plate boundaries are the main tectonic features for the Eastern Mediterranean tectonic setting. As a result of these tectonic movements, Anatolian Plate also has an inner continental deformation which creates mainly normal fault related the Western Anatolian Extension Zone.

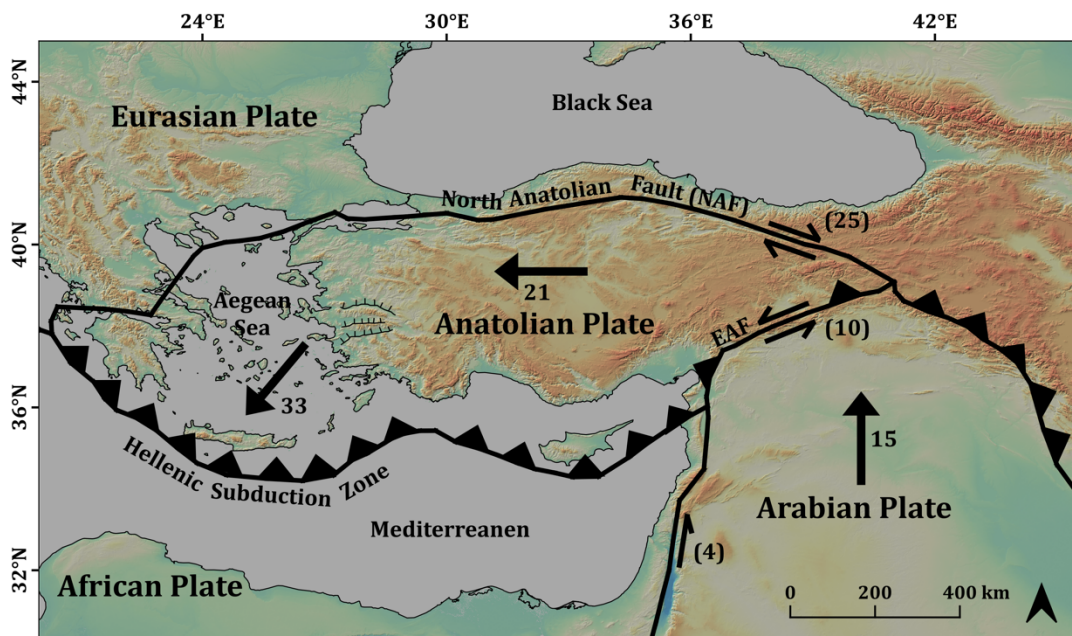


Figure 2.1: Tectonic setting of Anatolia and surroundings. Numbers show GNSS derived movement in mm/yr relative to stable Eurasia. Numbers in parenthesis show strike-slip fault rates. EAF is East Anatolian Fault. Slip rates and boundaries from [33] Reilinger et al., 2006.

2.1. North Anatolian Fault

North Anatolian Fault (NAF) is a seismically active ~ 1200 km long, right lateral strike-slip fault acting as a tectonic plate boundary. Since its discovery in 1948 by [23] Ketin, 1948, there have been numerous studies to unveil its mysteries. Especially the foreseeable behavior of NAF is one thing that intrigues geoscientists. It has been shown that every main $>M6.9$ earthquake on NAF is releasing the stress to next western portion of fault (Figure 2.2) ([37] Stein et al., 1997).

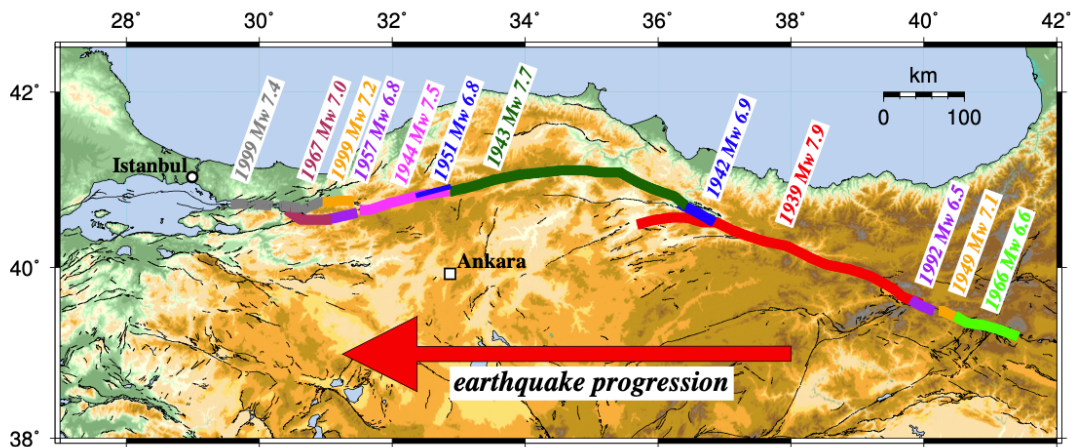


Figure 2.2: Earthquake propagation on the North Anatolian Fault. Notice earthquake events starting with 1939 M7.9, mainly transfers stress to next western segment. Figure from [20] Hussain, 2016.

The latest 2 $>M7.0$ earthquakes happened back in the year 1999 in Izmit and Düzce and ruptured a ~ 180 km long segment on the NAF ([20] Hussain et al., 2016). An earthquake is also expected on a particular NAF segment which is very close to the mega city Istanbul after these 2 earthquakes ([35] Sengor et al., 2005). The slip rate of NAF is 25 mm/yr which is close to slip rate of Anatolia (21 mm/yr [33] Reilinger et al., 2006.), which makes the strain on NAF is increasing everywhere on the fault. But every segment on NAF is in a different state in the seismic cycle since multiple creeping parts exist. Three main creeping segments on NAF can be seen on Figure 2.3. They're slipping without accumulating stress fully and mainly postponing earthquakes ([9] Bürgmann et al., 2000). Marmara segment is the submarine part of the fault which creeps partially ([7] Bohnhoff et al., 2017, [42] Yamamoto et al., 2019). Marmara segment is also the most hazardous segment of the NAF since it's very close mega city Istanbul. There have been some studies forecasting $> M7.0$ earthquakes in this section of the fault in next years ([6] Bohnhoff et al., 2013).

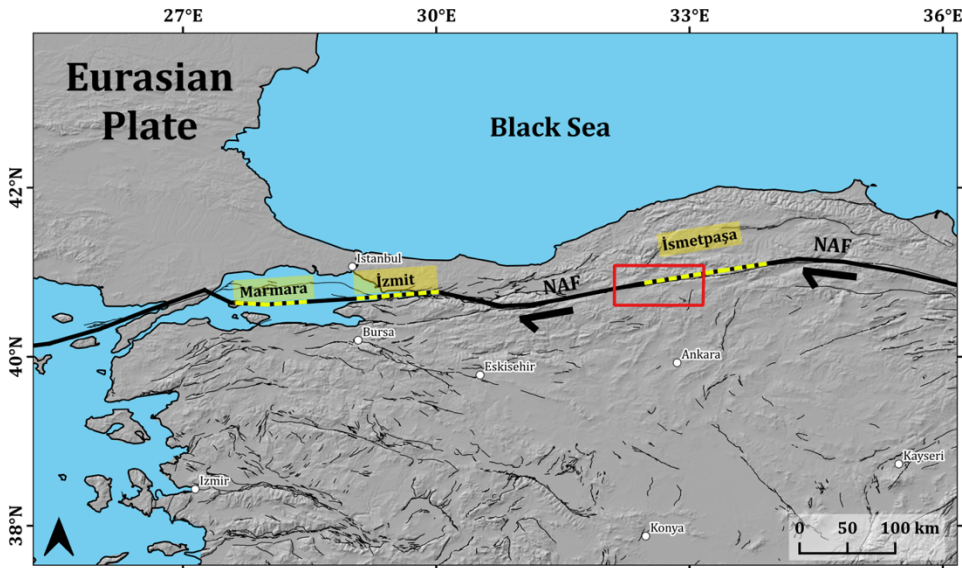


Figure 2.3: Main creeping segments of the North Anatolian Fault (NAF) shown with yellow dashed lines. Red rectangle shows the study area of this thesis. Faults from [17] Emre et al., 2018.

Apart from these known three segments, there are also some segments on Anatolia which is showing creeping clues on our datasets, for example Erzincan Segment of the NAF and Berendi fault in the Southern Turkey (see Figure 5.1 and Figure 5.3), but more studies needed on them. With advanced mm scale geodetic measurements, I believe more and more creeping segments can be found in Turkey. For the time-series part of my thesis, I will focus on behavior of certain parts on Ismetpasa Segment.

2.2. Ismetpasa Segment

Ismetpasa Segment is one of the creeping segments on the North Anatolian Fault with a length of ~ 80 km's alongside Marmara and Düzce segments. It has been discovered by [1] Ambraseys, 1970. He documented the surface creep rate as 20 mm/yr. He also noted the ambiguity of temporal extend of this event which happened in a period of 12 years, pointing out the unknown if these events happened gradually or transient. Later, a surface creep rate of 8 ± 3 mm/yr has been found by [10] Cakir et al., 2005. Then [5] Bilham et al., 2016 updated the creep rate as 7.6 ± 1 mm/yr and found out that the creep rate has been continuously decreasing since after two $>M7$ earthquakes on 1943-1944. However, there are still debates about creep rate decreasing, some say it could be related to 1999 Izmit and Düzce earthquakes ([20] Hussain et al., 2016). Also [12] Cetin et al., 2014 documented the strain release releasing every year is equivalent of a M5.1 earthquake.

The red rectangle in Figure 2.4 is the study area for this thesis. The Sentinel-1 LiCSAR (section 3.4) data has been downloaded for a broader LiCSAR product and clipped to this smaller and computationally easier to analyze area. Other reason is, it already has been published before that a specific profile in this clipped area (red rectangle) is showing behavior of transient slip ([34] Rousset et al., 2016). I also wanted to include a known “locked” portion of North Anatolian Fault (Western portion of red rectangle, with no yellow dashed line).

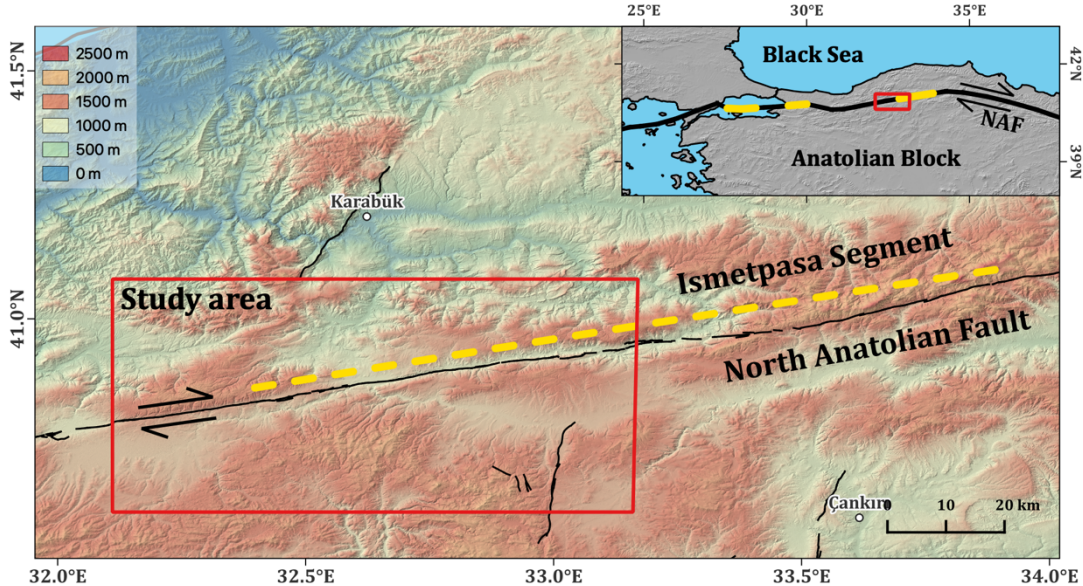


Figure 2.4: Study area of this thesis shown with red rectangle. Ismetpasa Segment has been indicated with yellow dashed line. Faults from [17] Emre et al., 2018.

My area is 4620 km² in size, positioning more to be in western portion of the whole North Anatolian Fault. It's a mountainous area with a semi-populated with vegetation. Especially northside of NAF in the study area could be considered as a forestland. South of it is more of an agricultural area. There is also normal fault related tectonic features in southeastern part in the study area ([17] Emre et al., 2018). But the focus of this work is the Ismetpasa Segment or to be more precise, small western portion of Ismetpasa Segment. There have been multiple ~M5.0 earthquakes happened very close to the segment, ~7 km in depth and around 30 km southeast back in September 2019 where we also analysis the data for. We didn't consider these earthquakes further in our study. More info on these earthquakes can be found out via the following link [2].

3. Data and Methods

I've used multiple software packages and multiple visualization tools to get my results. For high-resolution strain map I've calculated multiple equations involving filtered GNSS and filtered InSAR derived velocity raster. For my main time series analysis, I've used open-source InSAR time-series analysis package LiCSBAS which uses the images from LiCSAR portal. After corrections and filtering with LiCSBAS, I've run multiple Shell/Python/MATLAB scripts to create 3D time-series figures for my predetermined profiles. I've used multiple temporal slicing ways to fit the time-series data. Other datasets I've used other than mentioned in this section are SRTM30 DEM dataset ([18] Farr et al., 2007) and Turkey's faults database ([17] Emre et al., 2018). I will explain the details of my workflow in the next parts in this section.

3.1. Strain Mapping

Strain rate maps show the deformation rate on the surface of the earth relative to a stable area ([25] Kreemer et al., 2014). This enables observing plate motions on the surface of the globe. Generally, strain mapping is done with GNSS derived velocity datasets but in recent years InSAR derived strain rates were used more and more. I've started my analysis with high-resolution strain mapping for Turkey using both GNSS and InSAR derived data with a method developed by [31] Ou et al., 2022. The method is strong for its ability to preserve high-resolution deformation from the InSAR and strain rate tensor derivability from the GNSS method by combining them. This technique calculates several equations containing vertical GNSS velocity fields and down sampled/filtered LOS InSAR velocity raster. The strain map in the end can reveal creeping sections on a fault with its very high spatial resolution. It can also show potential places of unknown creeping areas and fault locations. I will further elaborate this in results (Section 4.1) and discussion (Section 5.1) sections.

3.2. SAR Interferometry

SAR Interferometry or more commonly known as InSAR is a geodetic technic using two (or more) actively sensed radar images to map the surface ([41] Woodhouse, 2017). A SAR image has two main components: phase and amplitude. The phase component is the

number of wave oscillations between the sensor and the surface. The amplitude is the intensity of the SAR wave. One SAR image doesn't give much info since the number of wave oscillations generally not known, but interferometry can compare those two (or more) images and give the meaningful info. If there is difference between those two images, InSAR can point it out with a millimeter accuracy. The spatial resolution of an InSAR image is directly related with the sensor wavelength ([41] Woodhouse, 2017). Sentinel-1, which has been used in this study, has a C – band sensor that can detect surface displacement differences in mm scales. An InSAR image (or an interferogram) can be seen in Figure 3.1. The closer fringes are to each other the more surface displacement occurred. Every fringe (~ 2.8 cm) shows the deformation in direction between the surface and the satellite sensor.

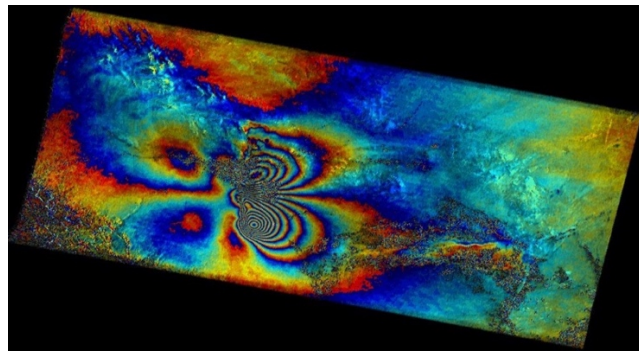


Figure 3.1: An example interferogram showing the deformation of 2003 M6.6 Iran-Bam earthquake. Fringes indicate the phase difference between the images taken before and after earthquake. Photo from ESA website [40].

I refer reader to these following books for more info on InSAR [16] [41]. Due to nature of radar wave, there is a lot of stuff going on between the signal, the atmosphere, and the surface. These all are the source of signal errors for InSAR. Below equation is a representative of this phenomena, showing the components of an InSAR measurement.

$$\delta\varphi = \delta\text{Orb} + \delta\text{Topo} + \delta\text{Def} + \delta\text{Atm} + \delta\text{Temp} + \delta\text{Noise} \quad (1) \quad [15]$$

$\delta\varphi$ in equation (1) is the total phase measurement. The signal required for a proper InSAR measurement interpretation is δDef , which is caused by surface deformation. To get desired deformation signal inside the total phase, the noise needs to be removed as much as possible. δOrb is the errors caused by satellite position. δTopo is the topographical errors, these signals can be mostly corrected with a proper DEM and known perpendicular baseline. δAtm is the atmospheric error generally caused by

tropospheric delays. Troposphere is the atmosphere layer closest to earth surface therefore it has a lot of moist. Moist together temperature and pressure they make the radar signal delayed in one (or more) of the InSAR images, therefore creates unwanted noise. $\delta Temp$ is caused by sudden “unwanted” changes on the ground between two images. $\delta Noise$ is all other noises in the InSAR signal, which is mainly quantified by coherence (0 - 1) meaning spatial correlation between pixels. Generally, as coherence gets bigger (close to 1), the noise gets smaller ([41] Woodhouse, 2017). Modern InSAR analysis packages can deal with most of these noises for most of the time with correct parameters (e.g., LiCSAR and LiCSBAS).

3.3. Sentinel-1

Sentinel-1 is a Copernicus program mission consists of multiple active radar satellites (currently two) launched back in 2014 starting with Sentinel-1A. The second of the series, Sentinel-1B, launched in 2016. The next Sentinel-1 satellites (C and D) will be launched in next ~ 3 years. Temporal resolution is directly related to number of operating satellites. So, until the launch of Sentinel-1B in 2016 the temporal resolution was 12 days, after 2016 it's increased to 6 days for most of the land on Earth. Sentinel-1 is a polar-orbiting, C-band SAR (synthetic aperture radar) satellite operating in all weather, day, and night. The Sentinel-1 data is open-source, providing high spatial and temporal resolution (6 - 12 days). It's a stable platform, enabling long-term time-series derivation like this study does. More info on the satellite, its mission and objectives can be found in Copernicus website [36].

3.4. LiCSAR

Since the Sentinel-1 launched in 2014, a need for scientific and systematic exploitation of the constellation occurred. Looking Into Continents from Space with Synthetic Aperture Radar (LiCSAR) ([26] Lazecký et al., 2020) has been developed in recent years to fill up this need because producing “number of” interferograms by oneself is one hard task especially from the computational aspect. LiCSAR is an automated workflow to produce standardized interferograms from Sentinel-1 images. The workflow includes producing geocoded interferograms and estimating coherences. The products in the end have ~ 100 m in spatial resolution. More info on the processing can be found on LiCSAR website [13]. LiCSAR is continuously processing new interferograms as new Sentinel-1 images are getting available. Since Alpine Orogeny is a priority for the LiCSAR workflow, whole Anatolia is getting updated often with new LiCSAR produced interferograms.

One of these frames has been shown in Figure 3.2 with the frame id 087A_04904_121313, the study area is clipped from this frame. Name of the frame id gives user some information about the frame. “087” is the orbit number of Sentinel-1. Next letter “A” is the acquisition geometry which is ascending. Following numbers are indicating location of the frame and number of bursts.

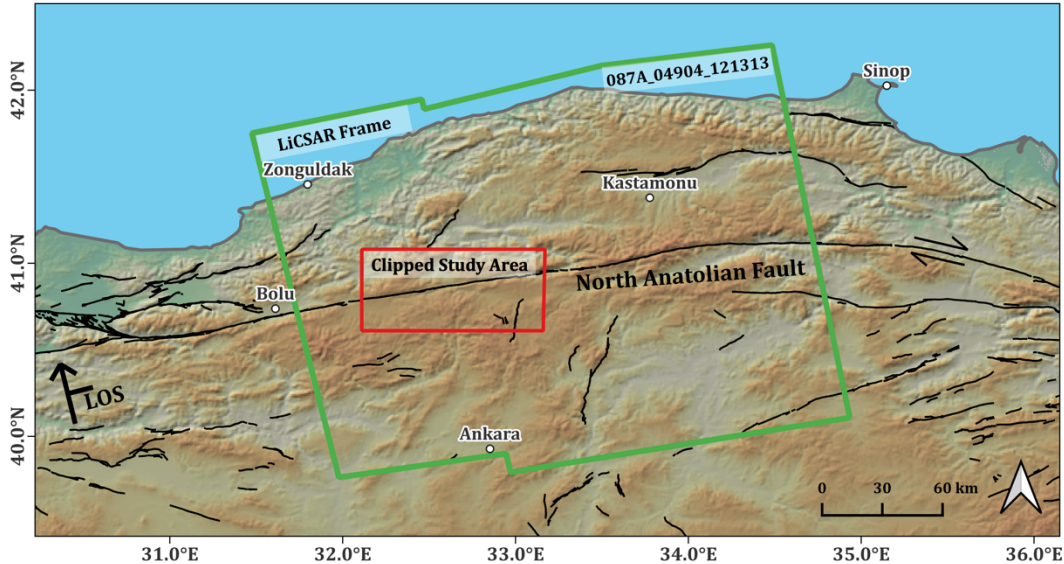


Figure 3.2: Study area clipped from LiCSAR ascending frame with the id 087A_04904_121313. The fault with the arrows is the North Anatolian Fault. Faults from Emre et al., 2018.

3.5. LiCSBAS

InSAR time series formation from SAR satellites like Sentinel-1, is a time-consuming and computationally intense work. LiCSBAS ([29] Morishita et al., 2020), by using a set of already available LiCSAR products, can generate a time series of interferograms with \sim mm/yr accuracy for big scale areas. LiCSBAS is semi-automated, open source, Python and Unix Shell (bash) based InSAR time-series software package. Since it does use already processed LiCSAR interferograms, LiCSBAS only deals with the time-series aspect (creation and analysis) of it. The workflow of LiCSBAS can be found in Figure 3.3. There are two main parts in LiCSBAS workflow. The first part deals with the preparation of LiCSAR data. It downloads the unwrapped interferograms and coherence values from LiCSAR web-portal, converts the data format (and down samples if enabled by the user), clips the data (if enabled by the user), and applies atmospheric correction (if enabled by the user). The result afterwards, sent to the second part for time-series analysis.

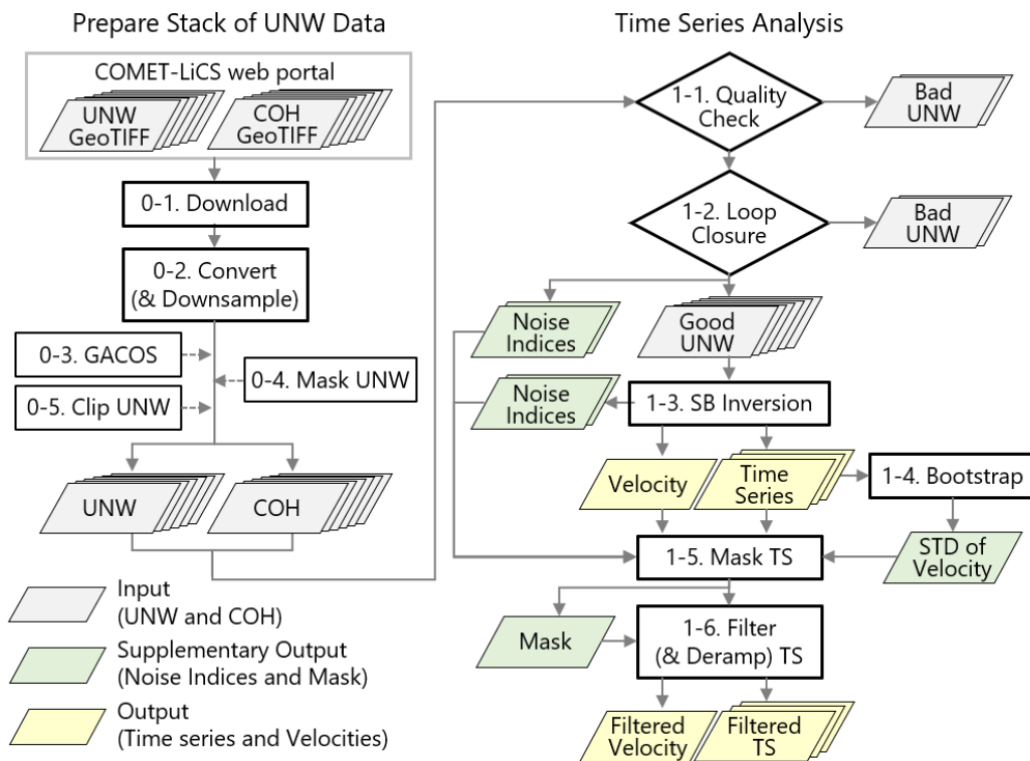


Figure 3.3: Two main parts of LiCSBAS workflow can be seen on left and right sides.
Figure from [29] Morishita et al., 2020.

The second part of LiCSBAS starts with quality checks. By both checking the coherence and unwrapped interferogram pixels if they're valid, LiCSBAS removes the bad pixels. The second, more comprehensive quality check occurs when the loop closure method (network refinement) starts. LiCSBAS in this step, does a set of calculations for the individual interferograms on the network and removes problematic ones. This is an image-by-image error correction not a pixel-by-pixel. After these two steps, "bad" interferograms are separated from the "good" ones, meaning on the next step the input will be only the "good" unwrapped interferograms. After separation, SB Inversion starts, and this step is the most computationally intense one. LiCSBAS applies NSBAS method ([27] López-Quiroz et al., 2009) for the temporal correlation of the time-series, which is a proper way to use InSAR time-series data in long-term slow slip study such as this thesis. The next steps on LiCSBAS workflow mainly deals with filtering, masking, and error mitigation.

I've downloaded and processed 872 interferograms from 261 images/dates with LiCSBAS for a period between 10.11.2014 and 23.06.2020. 5 images and 78 interferograms have been deleted due to errors and inconsistencies. More images for my individual profile have also been deleted, more on appendix section. I've made the

atmospheric corrections with GACOS ([43] Yu et al., 2018) step, more on this in next section. I've clipped the data (Figure 3.2) for mainly computational reasons. Clipping extend was chosen to be a stable (visually checked throughout the time-series), non-forested, mostly flat relatively small area (Figure 4.1). I've applied mask after SB inversion step, with different thresholds applied for different parameters, 40.9% of the pixels are removed in the final dataset by the mask. Figure 3.4 shows the full-extent, perpendicular baseline of the network. Perpendicular baseline is the perpendicular distance between two satellite sensors for one interferogram which consists of two individual acquisitions. There is only one gap in network which is late 2016.

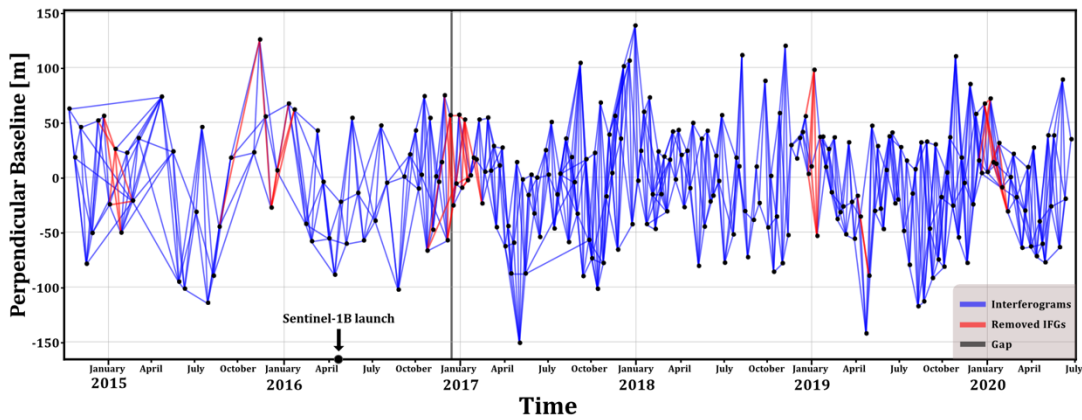


Figure 3.4: Perpendicular baseline for the study area, meaning relative spatial position of the Sentinel-1 sensors in space/time for each image. Notice how Sentinel-1B launch in April 2016 made temporal resolution increase significantly.

3.6. GACOS Atmospheric Correction Service

Atmospheric delay in InSAR images can make the valuable deformation signal masked or all together wipe off, thus harder or impossible to interpret. So, the delay should be removed as much as possible. Therefore, GACOS (Generic Atmospheric Correction Online Service) has been developed by [43] Yu et al., 2018. GACOS use operational data from ECMWF (European Centre for Medium-Range Weather Forecasts), and continuous GNSS atmospheric delay estimates to calculate atmospheric delay corrections for InSAR. For my time-series, ~4.5 years of GACOS data was already available to apply in LiCSBAS workflow step 0-3 (Figure 3.3). For the rest of the time-series, between 08.22.2019 and 23.06.2020, I've specially requested GACOS data for every specific image date I have, 48 of them.

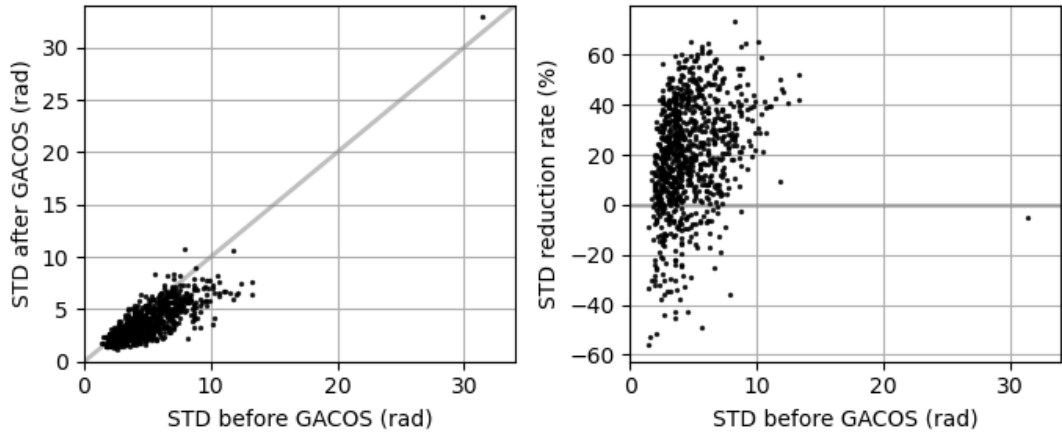


Figure 3.5: Impact of GACOS correction. The left panel shows before and after standard deviation distribution of interferograms. Right panel shows reduction rate for each interferogram.

3.7. Time Series Analysis

I've created a time-series between 10.11.2014 and 23.06.2020. To detect LOS (line-of-sight) creep-burst or slow-slip events (SSE), not a “pixel” time-series but a “profile” time-series is needed. Therefore, I've prepared several 3D time-series for the study. To make this possible, I've determined multiple profiles to show deformation evolution in 3D, both for locked and creeping parts of NAF. These profiles are 8 km long, 1 km (half-swath is 0.5 km) wide rectangles. Crossing NAF right in the middle (at 4th km). For 3D time-series I've produced all possible interferograms from the first date to last date with the temporal separation 6 to 12 days (rarely more than 12 days) between each. Especially before Sentinel-1B launch, temporal resolution was relatively low. In the end I had 255 interferograms. I made a proper time elongation for the time axis, this way it was possible to see increasement of the temporal resolution. Moreover, I prepared 2D time-series showing evolution of multiple pixels derived from 3D time-series. I've extracted 2 2D plots from each side of the fault from 3 average values (each average value is an average of ~16 values) centered at ~300 m swath and with a same distance to the fault, compared them and find the difference between them. This enabled a simple but persistent error correction. This way it was possible to detect any creep jumps. For the standard deviation of the difference plot, I've used simple error propagation ([32]). Furthermore, I've applied temporal slicing (3 and 6 months) to the 2D data and made a linear fit in-between each slice. I also found the sudden change points in the signal with the method by [24] Killick et al., 2012, then applied a linear fit to data.

4. Results

~6 years of Sentinel-1 data with the extend of the study area have been processed with LiCSBAS package. The data has a spatial resolution of ~100 meter which is a limitation comes from LiCSAR produced images. The spatial resolution however is relatively high, between 6-12 days for the most part. There were some images that have been deleted, more on this can be found in appendix. Figure 4.1 shows pre-selected LOS (line-of-sight) cumulative displacement date pairs, which are corresponding to ~yearly cumulative LOS deformations. Small blue rectangle shows the reference area which has been checked visually and selected to be a stable one.

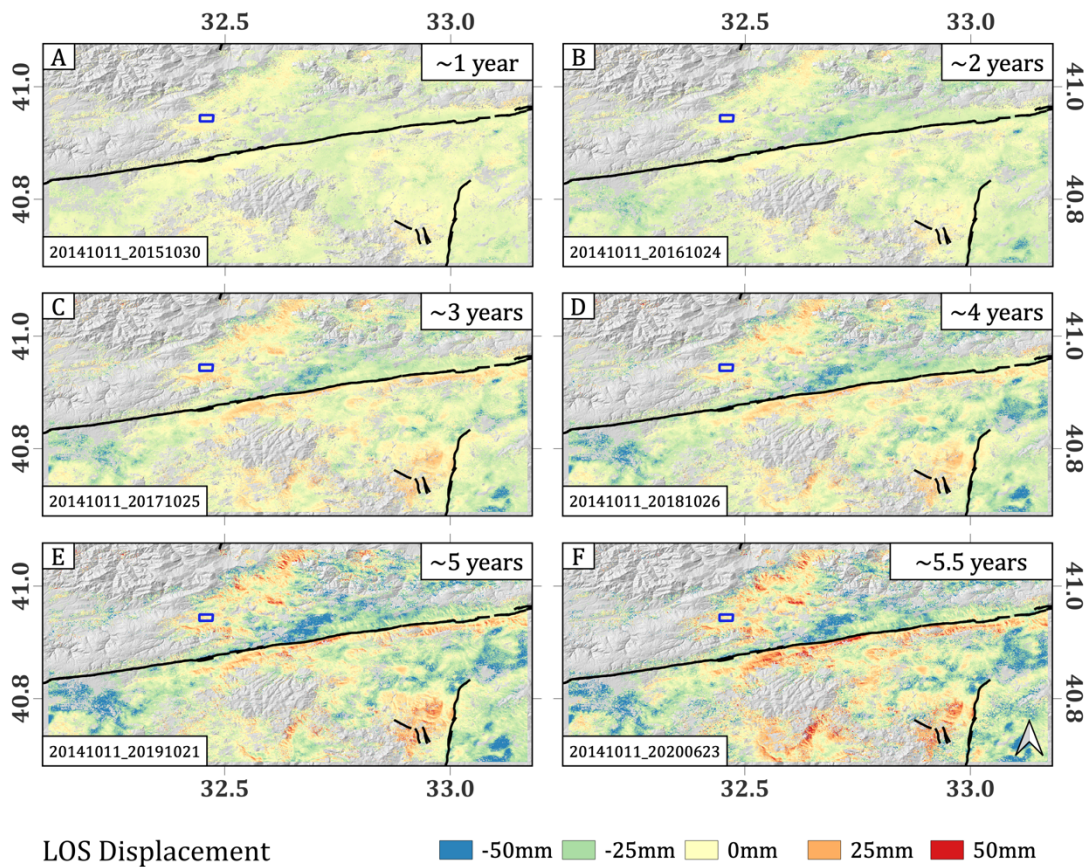


Figure 4.1: Evolution of tectonic deformation in the study area. Starting with panel (E), topographic signal can be seen which assumed to be error and further disregarded in following analysis. A linear deformation assumed to be tectonic signal can be seen along the North Anatolian Fault. Blue rectangle shows the stable reference area.

4.1. High-Resolution Strain Map for Anatolia

High-resolution filtered velocity fields derived from InSAR and GNSS have been used to get high-resolution strain map with the method explained by [31] Ou et al., 2022. By comparing results with the [39] Weiss et al., 2020, high-resolution strain map on the left panels looks sharper, but right panels look more smoothed out (Figure 4.2). There are many high-strain parts in the new raster which cannot be seen in the old method. So, with this kind of a high-resolution strain map, it could be possible to detect unknown faults and creeping areas. This will be more elaborated in the discussion section.

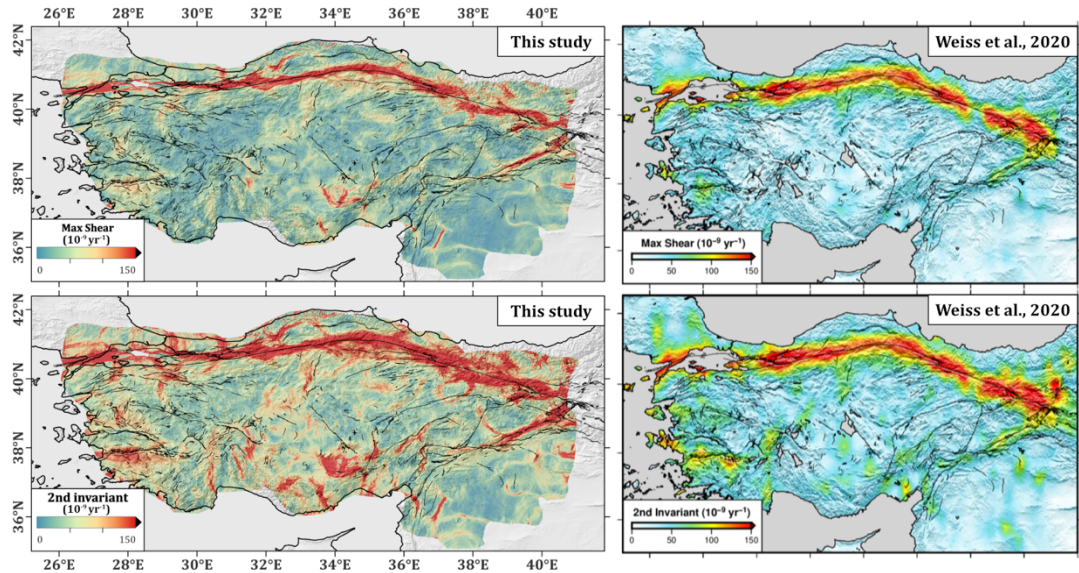


Figure 4.2: Comparisons between [39] Weiss et al., 2020 and this study's high-resolution strain rates. Sharper strain rates can be seen on the left panels. 10^{-9} yr^{-1} is nano-strain.

4.2. Profiles on NAF

Pre-determining the profiles to use in 3D plots is crucial since the time-series plots entirely rely upon them. Therefore, looking at Figure 4.1, 3 profiles showing 3 different deformation patterns have been chosen to show all the aspects of the dataset (Figure 4.3). The first profile, profile (a) shows the locked portion of the NAF. It is assumed to be showing small amount of tectonic deformation in time, since it's outside of Ismetpasa creeping area. The second one (b) is the main profile I've done my most analysis on in the discussion section. A creep movement has been known to be taking place there for a long time.

The (b) profile is also the same profile with what [33] Rousset et al., 2016 have been used for their figure 3 (Figure 1.4). Third profile (c) is another creeping area chosen by interpreting Figure 4.1 images. Each profile in Figure 4.3 is an 8 km long, 1 km wide, NAF-perpendicular rectangle.

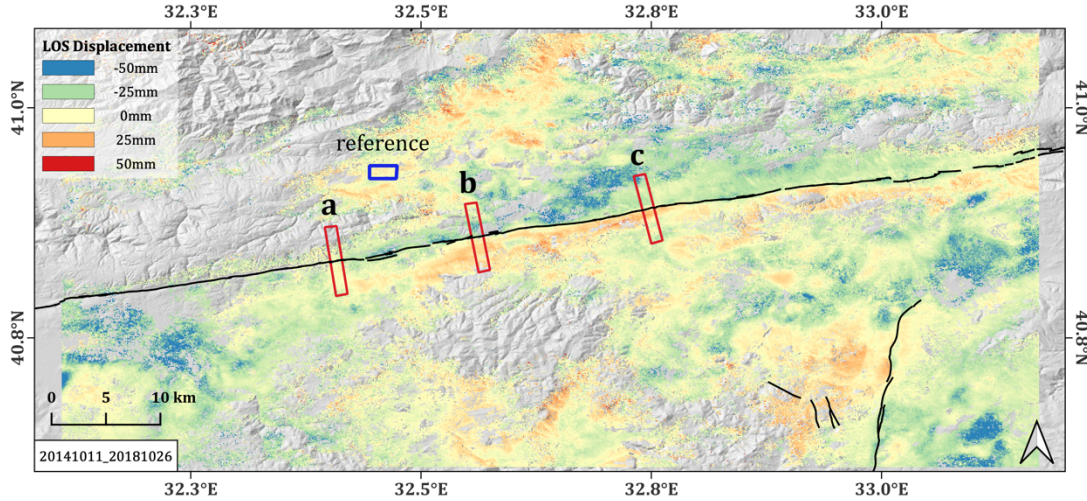


Figure 4.3: Three 8 km * 1 km profiles used in this study. Profile (a) is on locked portion, profile (b) and (c) are on the creeping portion on the North Anatolian Fault. The blue rectangle shows the reference area for the raster. Faults from Emre et al., 2018.

Elevation of profiles can be seen in Figure 4.4. High elevation on the Northern part of profile (a) is masked by the LiCSBAS. Profiles (b) and (c) don't vary as much as profile (a). There doesn't seem to be a correlation with displacement signal and elevation, especially after masking from LiCSBAS.

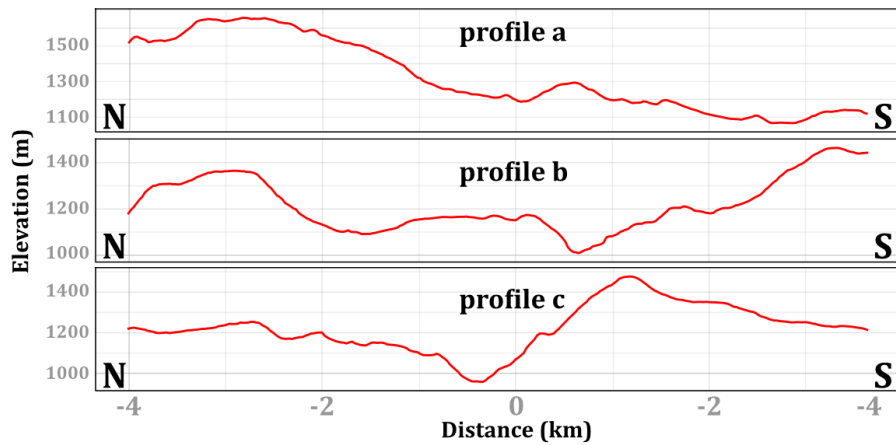


Figure 4.4: Elevation of profiles (a), (b) and (c) on the North Anatolian Fault.

Pixel sizes are ~100 meters but the analysis have been done using a step size of 150 meters. Therefore, for every set of width pixels have 16 pixels and every set of length pixels have 55 pixels. So, each rectangle profile has maximum of 880 scatters/values. If there are masked pixels in one of the images in date pair, it won't be shown in the plots. Figure 4.5 shows a simple view of each profile size. After determining the profiles, a 3D time-series plot has been made, which shows each possible cumulative displacement file (date-pairs) starting with a reference image of 20141011. Every cumulative displacement file has the same reference image, the first one being 20141011_20141023 and the last being 20141011_20200623. To get each displacement profile, several scripts has been run.

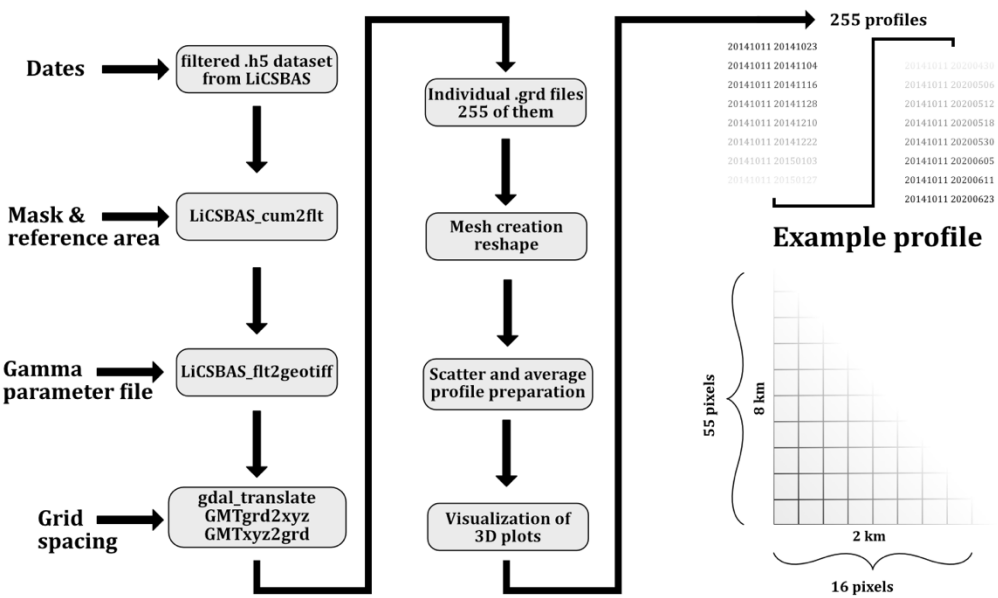


Figure 4.5: A schematic view of automated way of creation of individual cumulative displacement files and an example profile size.

The main cumulative displacement raster preparation has been done with a shell script (which can be found in appendix) for all possible dates, 255 of them (Figure 4.5). Inside the script, 2 LiCSBAS functions (LiCSBAS_cum2flt.py and LiCSBAS_flt2geotiff.py) have been used to get cumulative displacement as a GeoTIFF file. Reference area in the clipped raster and the mask that LiCSBAS already calculated has been applied in this step. To prepare the scatters, a certain filetype (GMT NetCDF grid file) is needed for further analysis. So, after 2 LiCSBAS functions, GeoTIFF files need to be converted to grid files. This is done with multiple GMT and GDAL scripts. In the end, a cumulative displacement grid file has been created for each date pair.

A sample scatter profile has been shown in Figure 4.6. It shows the LOS deformation between the dates 20141011 and 20180914. Each scatter in the plot has 5 parameters. These are distance along profile (km), distance perpendicular to profile (km), original longitude, original latitude, and the LOS deformation value (mm).

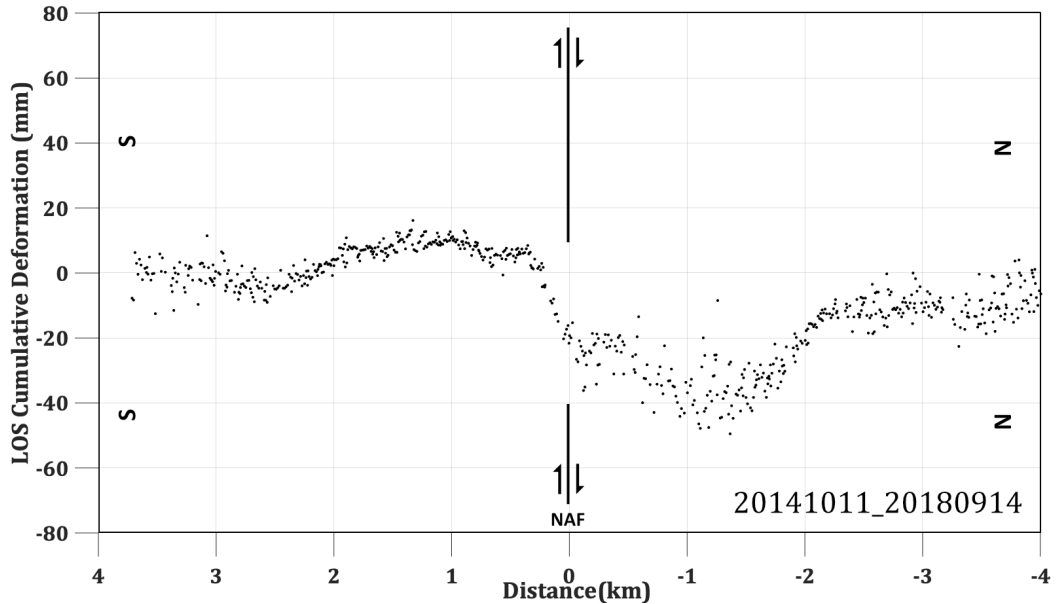


Figure 4.6: An example of cumulative displacement scatter points for one date pair for profile (b). There are 707 scatters out of 882 (normally) in this plot. The rest are masked for this individual date pair.

4.3. 3D deformation time-series for the NAF

After preparing all the 2D scatter plots like Figure 4.6, I have checked and removed the outlier date pairs (scatter profiles) from the time-series. For plot (a) 2, for plot (b) 3, for plot (c) 5 of date pair cumulative displacement file have been manually removed from the following figures and analysis after visual control. Manually removed data pairs for all three plots further explained and showed in appendix (Figure A.1). 3D scatter plots are showing the same area for a period, it's the temporal evolution of an area. Therefore, one of the tricks is the time axis. Since some dates are removed by LiCSBAS, there are gaps in time series. Also, before Sentinel-1B launch in April 2016, temporal resolution was at best 12 days, sometimes lower than that. For plotting these grid files in a time axis, a certain properly spaced date list has been created. For visualization, only the month and year of the later date has been selected, the day difference hasn't been shown. Figure 4.7 shows the temporal evolution of the profile (b) in a ~6 years period. North Anatolian Fault is at the distance "0".

South side of the NAF is showing a positive deformation meaning south side is moving westward, therefore getting closer to the satellite in LOS direction and vice-versa for the Northern side. This is expected for an ascending scene of Sentinel-1.

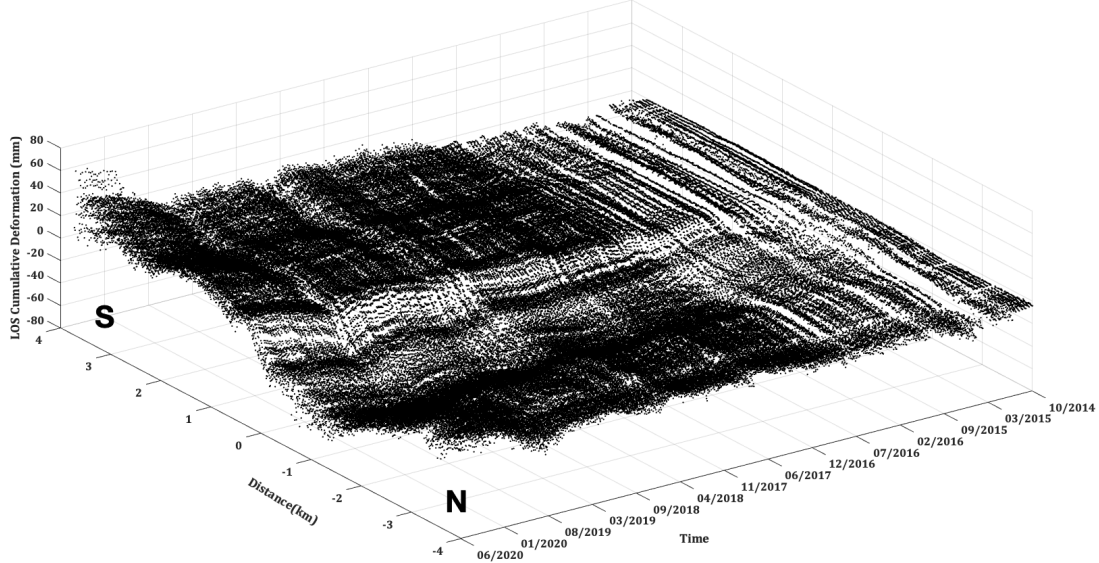


Figure 4.7: Scatters of 255 interferograms starting in 2014. Evolution of the profile (b) between 10.11.2014 and 06.23.2020. NAF is at km “0”. Reference date for all date pairs is October 14th, 2014.

More statistics can be extracted from each of data pairs. These are simply averaged for every step size. Since the profiles are 8 km long, there will be 55 (8 km (profile length)/0.15 km (step size)) average values for every profile (a, b, and c). These include average distance along profile (km), average longitude, average latitude, average LOS deformation value (mm), standard deviation of values, minimum of values, maximum of values and number of scatters in the step. Figure 4.8 shows temporal evolution of the profile (b) in ~6 years. Red lines are the average values for each set of scatters in step size (150 m).

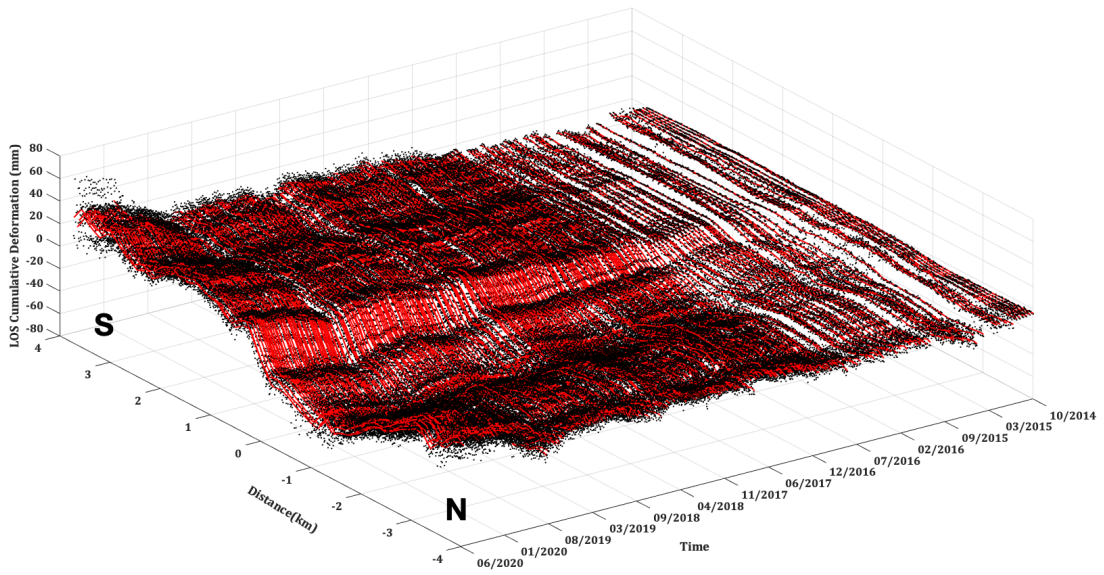


Figure 4.8: Evolution of creeping profile (b) in ~6 years with red lines showing the average positions of scatters.

Figure 4.9 shows the profile (a) temporal evolution. This profile is on a locked portion of the NAF (see Figure 4.3). The removed area between the km's -4 and -2 are the masked/removed pixels by LiCSBAS due to topography. Profile (a) is at ~12 km West of profile (b).

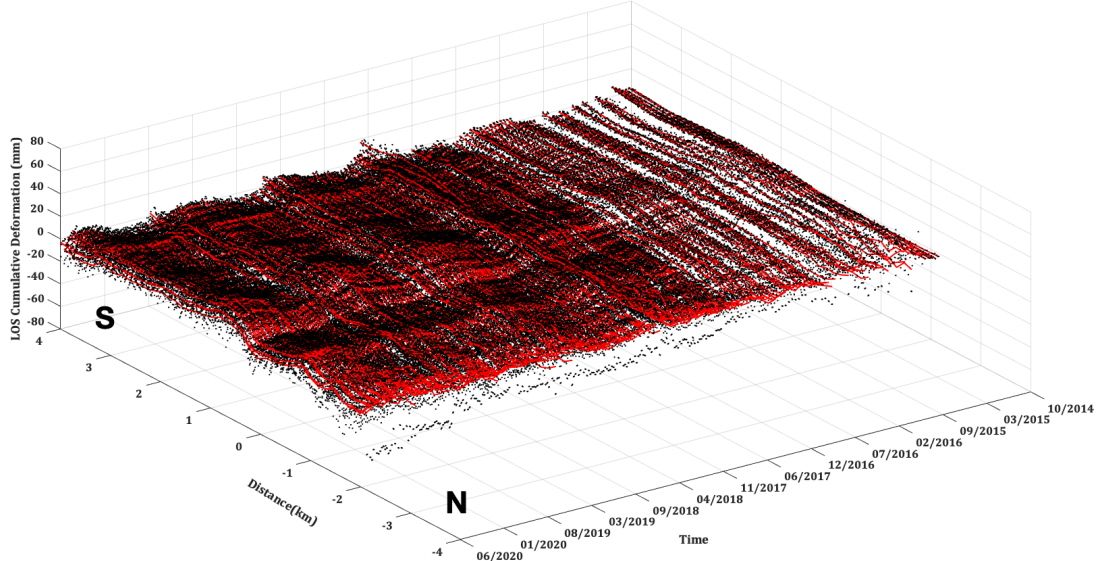


Figure 4.9: Profile (a) temporal evolution for ~6 years. This is a “locked portion” of the NAF.

Temporal evolution of profile (c) can be seen in Figure 4.10. Profile (c) is at ~15 km East of profile (b). Creep can be clearly seen in the time-series.

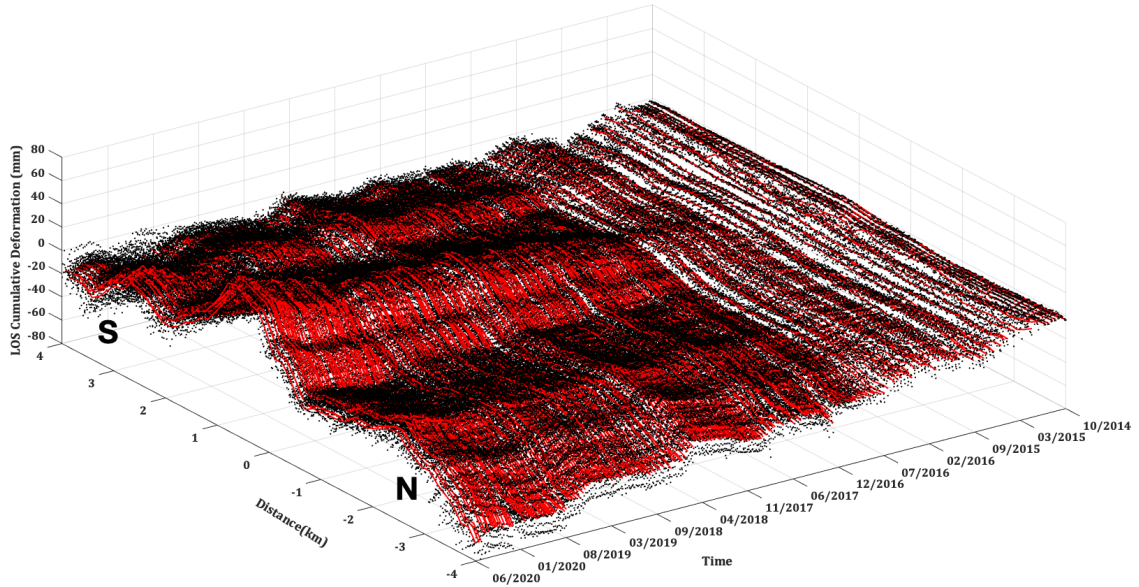


Figure 4.10: Temporal LOS deformation evolution of creeping profile (c) in ~6 years.
This is a creeping section of the fault, like profile (b).

4.4. Temporal evolution of a swath in time-series

Average line-of-sigh (LOS) deformation change can be visualized by taking swaths from either side of the fault from the 3D time-series (Figure 4.11). Both fault parallel swaths (blue and orange) are centered at 300 m distance, meaning 3 average values in distance (distance between first and third average value is ~300 m (with 150 m step size)) used. Figure 4.11 shows the approximate swath location which is ~500 m apart from each other (~250 m from the fault). The green line is simply the difference between other two lines, blue and orange. Multiple analysis with multiple time series will use the green line for all the profiles continually. Blue line is on the south side of NAF which moves to Westward (positive values), meaning getting closer to right-side-looking ascending satellite. The orange line is on the Northern hand side of the NAF, showing negative values meaning getting farther away from the satellite.

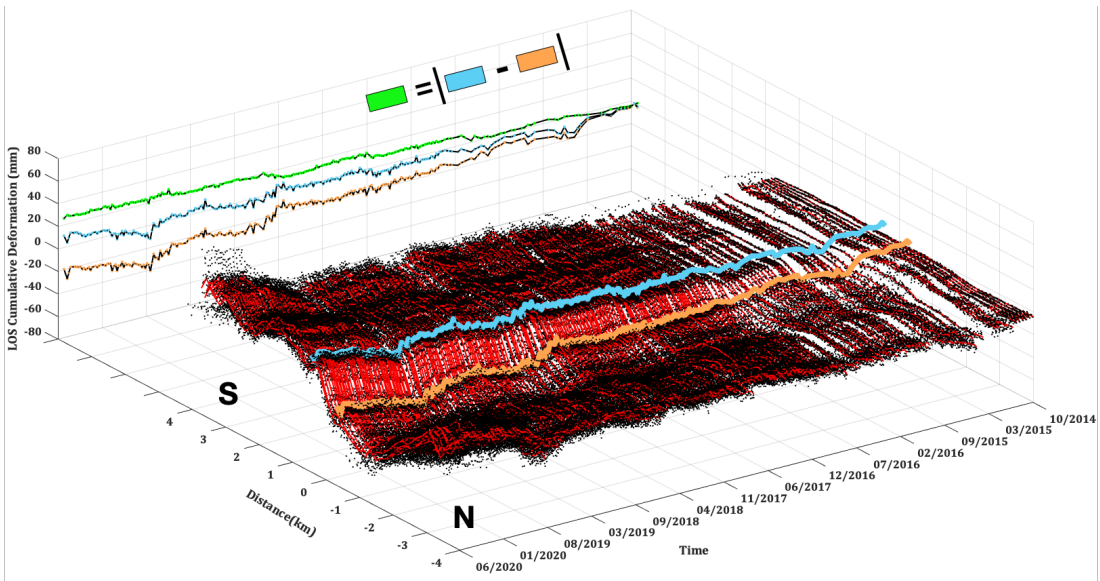


Figure 4.11: Time series for LOS deformation for profile (b). Blue and orange lines are showing the mean value of a swath centered at ~300 meters. Blue and orange lines are ~500 m apart from each other. Green line is the difference between blue and orange lines.

Like mentioned in the previous section, it's also possible to extract standard deviation using scatter values for all the date pairs (Figure 4.12). The standard deviation for each line shown with transparent error envelope around the lines. The error envelope for the green line was done with a simple standard deviation error propagation shown with equation (2). Δ is the standard deviation.

$$\Delta_{green} = \sqrt{(\Delta_{blue})^2 + (\Delta_{orange})^2} \quad (2) \quad ([32]$$

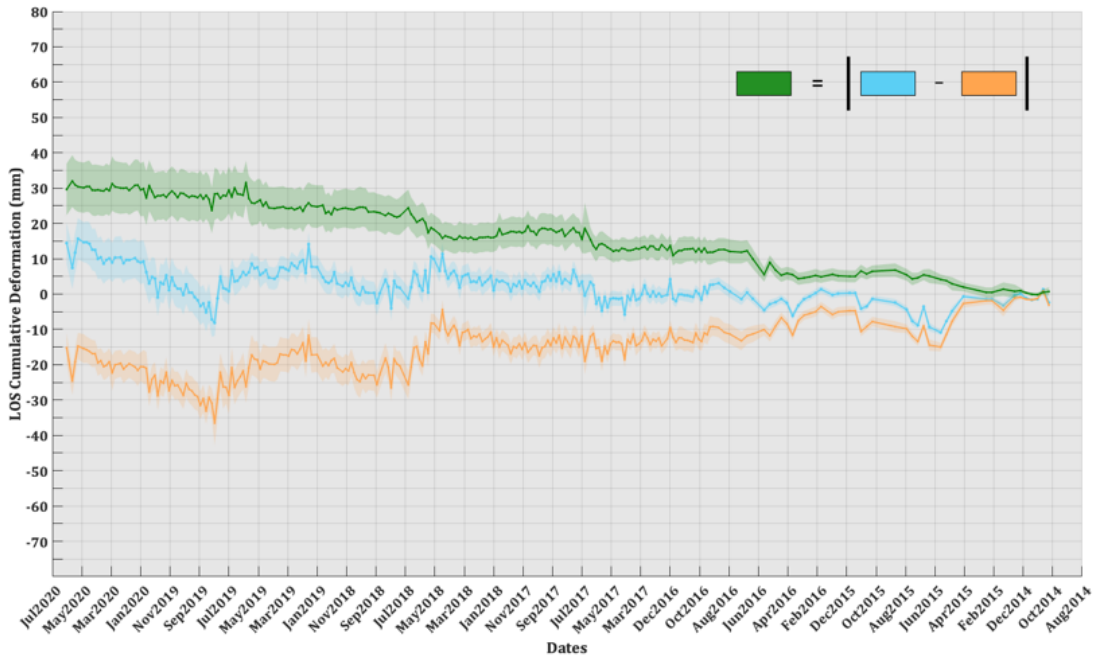


Figure 4.12: Temporal evolution of profile (b), with the error envelopes. Blue line is taken from a swath from Southern part of fault. Orange line is from Northern part. Green line is the difference between orange and blue lines. Error envelope around the green line is the result of simple error propagation.

Since the blue and orange plots are showing each side of the NAF, calculating the difference between them in time acts as a simple but powerful way to noise removal. As an example, high fluctuation can be seen in Figure 4.12 after March 2018 on blue and orange lines, but the green line is mostly linear. This is due to the same noise source has been affecting both sides of the fault in temporal and spatial scale, but the difference is mostly the same, so the green plot is not fluctuating as much as the other 2 plots.

5. Discussion

5.1. Creeping areas derived from strain map

High resolution strain maps have an importance in seismic hazard estimation and better understanding of fault mechanisms. They indicate deforming areas which makes it very beneficial for long term slow slip sourced deformation. In contrast to Figure 4.2, strain rate map on Figure 5.1, now shows most deforming areas in red patch with a fine-tuned color bar. I've selected 4 parts on the North Anatolian Fault visually, to take a closer look to them. Red patches in Figure 5.1 shows areas with high-strain rates.

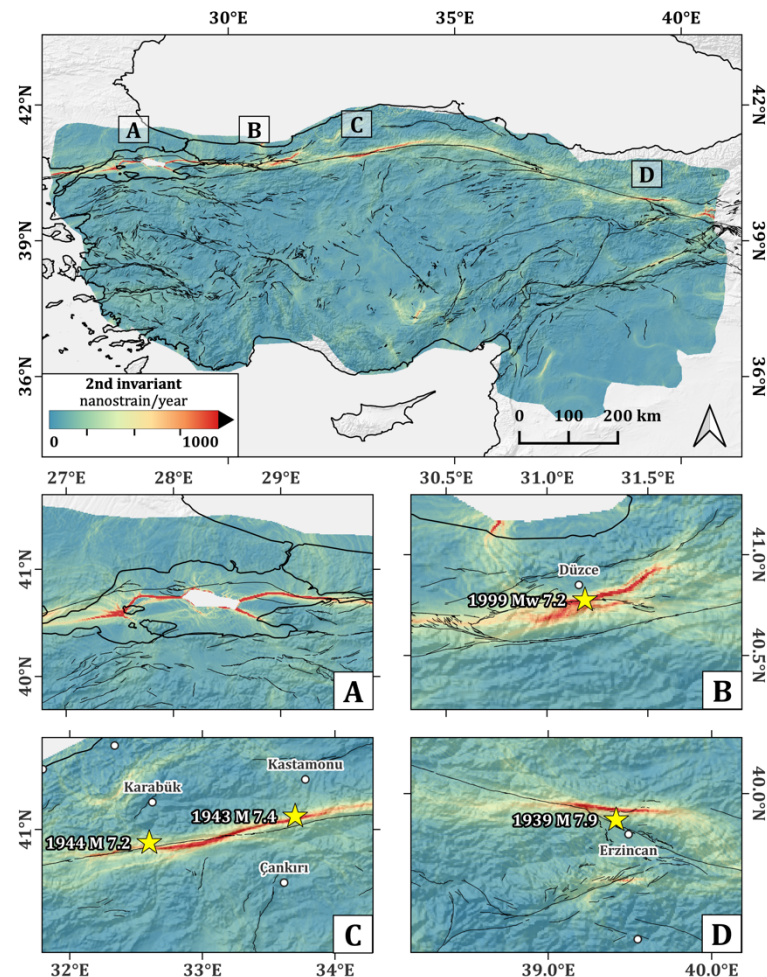


Figure 5.1: High Resolution strain map for Anatolia. A, B, C and D shows certain parts of NAF. Red rectangle in panel C shows the focus of this thesis. Faults from [17] Emre et al., 2018.

Focused areas (A, B, C and D) show that high-strain parts are “mostly” correlated with known creeping sections. This indicates the possibility of a use strain rate maps for creeping area detection. In addition, [31] Ou et al., 2022 have developed and used this method to identify a creeping section on Haiyuan Fault in Central Asia. Out of these 4 areas, 3 of them (A, B, C) is right on documented, well-known creeping areas. Panel A shows the offshore Marmara Segment of NAF, the filtering method manages to interpolate offshore strain, but more studies needed for the method to work properly in offshore. This portion of NAF is known to be a creeping segment of the fault ([7] Bohnhoff et al., 2017, [42] Yamamoto et al., 2019)). Red patches in Panel B are showing the Düzce segment of the NAF. High-strain field has been shown to be creeping by [20] Hussain et al., 2016. It’s a ~50 km segment according to my results, but the extension of high-strain field is stretching to an unknown fault on ~20 km Northeast of Düzce Segment. So, the results are not perfectly overlapping with the known faults of Turkey from [17] Emre et al., 2018. Indicating either the method needs more work, or some additional studies needed to identify creeping areas. Panel C has Ismetpasa Segment inside where this study is focusing on. Ismetpasa Segment extension is almost perfectly overlapping with the result. Spatial extension ~80 km has been found by [10] Cakir et al., 2005. In my results it was extending to ~100 km’s. I will elaborate more on this high-strain area in next sections of my study. Strain profile for Ismetpasa Segment can be seen in Figure 5.2.

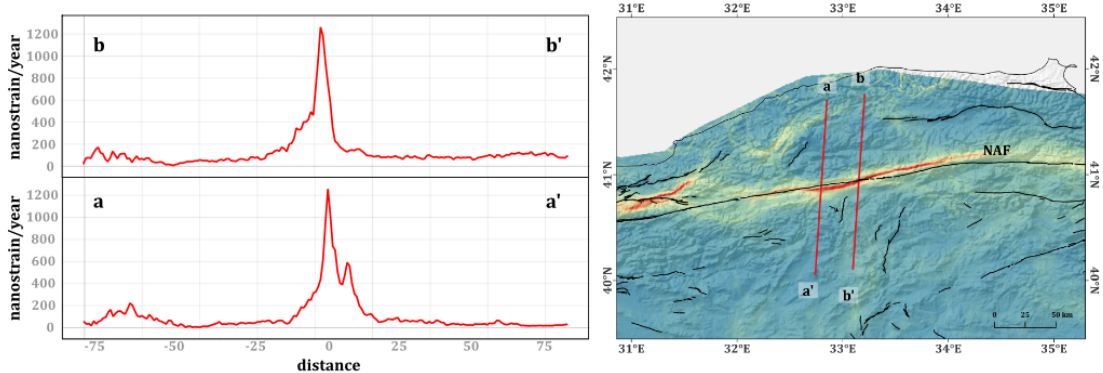


Figure 5.2: Strain profiles on the Ismetpasa creeping segment on Northern Anatolian Fault.

Finally, panel D red patches have a potential to be an unknown creeping area (to my knowledge). It’s starting from main part of NAF then extends to East, Northern part of Erzincan Fault. The length of this part is ~45 km. Also, the patch here almost perfectly overlaps with the epicenter of 1939 M7.9 Erzincan Earthquake calculated by [14] Dewey, 1976 ([3] Barka, 1996) which 10 km NW of Erzincan, indicating that a possibility to be a postseismic creep starting in with 1939 Earthquake. Other than creeping parts on the

NAF, there are 2 more high-strain areas that needs to be further investigated. These are shown in Figure 5.3, one area is on the Eastern Anatolian Fault (EAF) the second one is in Central Southern part of Turkey. Distance of high-strain part on the left panel of Figure 5.3 is ~ 40 km and it could be started creeping after 2020 Mw 6.8 Elazig Earthquake. Right panel shows another deforming area which is ~ 23 km in distance, which is happened to be on a Berendi Fault, but the strain and fault doesn't seem to be correlated. In any case, this high-strain areas should be further investigated. In my knowledge there is no reported creeping for Panel D in Figure 5.1 and two areas in Figure 5.3.

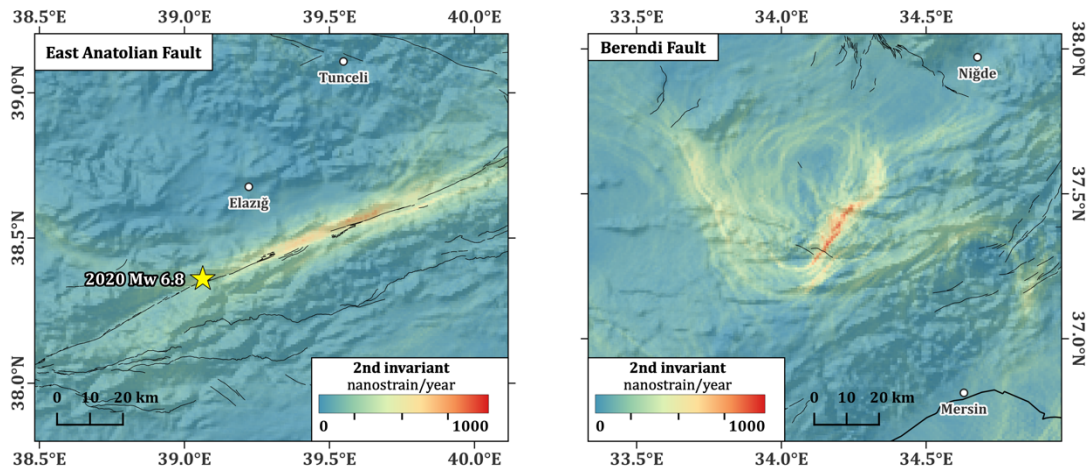


Figure 5.3: Two other areas that is showing 1000+ nst/year. Source of deformation on left figure could be 2020 Mw 6.8 Elazig Earthquake. High-strain field on the right is on Berendi Fault but not correlated with the fault. Faults from [17] Emre et al., 2018.

5.2. Locked vs creeping section of the NAF

Before any sleep-burst estimation, it's crucial to compare some 3D cumulative displacement time-series for checking signal consistency and any additional error throughout area of study. Figure 5.4 shows time-series for both locked part, profile (a), and a creeping part, profile (b), of the Ismetpasa Segment.

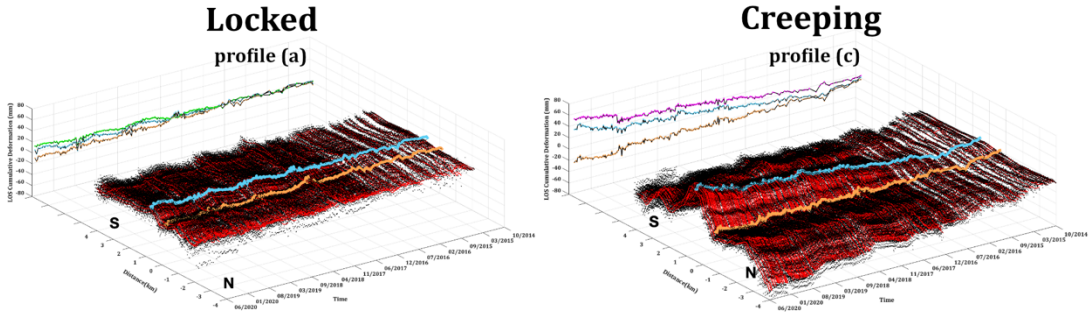


Figure 5.4: Profile (a) “locked” and (c) “creeping” evolution in ~6 years with temporal change. Green line and magenta line are showing the difference between their corresponding blue and orange swaths.

Several date pairs have been removed from these two plots of time-series, they can be found in the appendix section. Temporal evolution plots from both profile (a) and (c) has been shown to indicate differences between locked and creeping parts of the NAF. Green and magenta lines show the difference between their corresponding sides of the fault. Both swaths in both locked and creeping plots are taken from either side of the fault with a swath centered at ~300m. For both time series, maximum change between orange and blue lines considered, meaning swaths are taken visually where maximum change between orange and blue lines are expected. So, for the locked one the distance between orange and blue lines is ~550 m, for the creeping section it is ~900 m. Since the deformation mainly happens and extends to a bigger area, the ~900 m of main deformation area is understandable on the creeping section. ~2 km portion of the locked Northern part has already been removed by LiCSBAS, therefore it's masked in Figure 5.4. The comparison between green and magenta lines are shown in Figure 5.5. These are profiles (a) and (c) which has been already showed in Figure 5.4. Locked (green) line is starting from a difference of 10 mm LOS cumulative deformation and throughout the time-series stays around 10 mm level. This shows there is no or small difference of deformation between either side of the fault for the locked (green) line in ~6 years of time-series. Magenta line shows the difference between either side of the fault for profile (c). In contrast to green line, magenta line is showing higher rate of deformation in time. It's showing ~7 mm/yr of LOS deformation. Figure 5.5 shows locked and creeping parts together. Green line is showing seasonal oscillations indicating a possible deformation due to ground water. Magenta line seems to be showing no seasonal oscillations and seems to be creeping without any jumps.

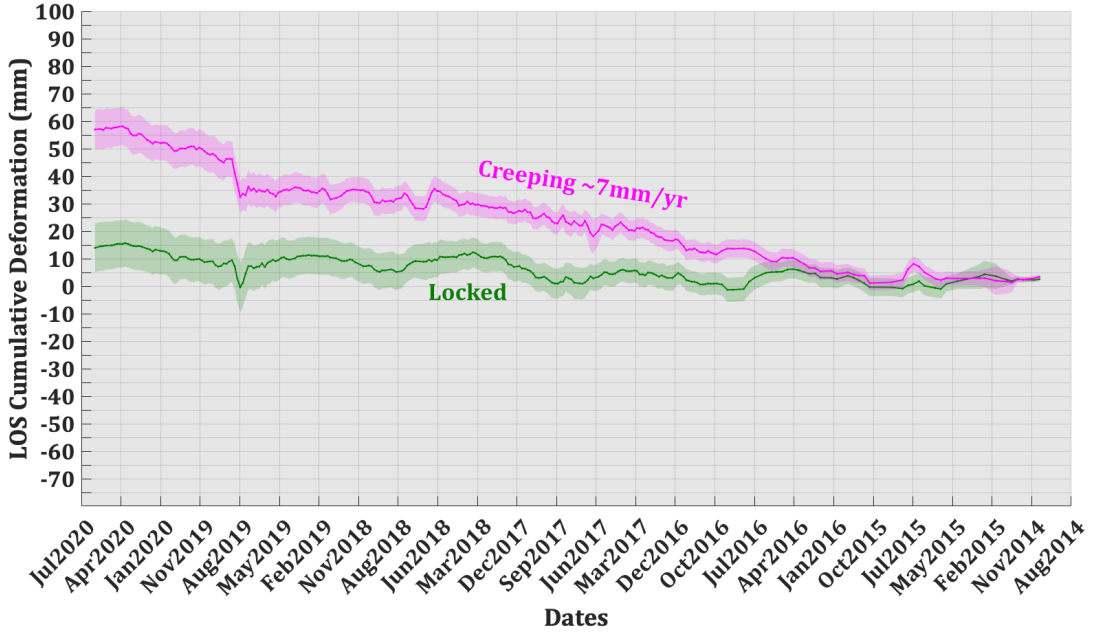


Figure 5.5: Comparison of differences between creeping and locked sections.
Creeping section is profile (c), locked section is profile (a).

Moving mean with 3 elements ($k = 3$) has been used for green and magenta lines for further smoothing the lines in Figure 5.5. General pattern is the same with non-moving mean used lines. There are couple peaks in signal (e.g., August 2019) which I've assumed to be noise affecting both plots. This is probably not a topographical or troposphere sourced error, but an analysis caused. Since these are two different places (~ 27 km's between them), I assume this is an over correction of the data after August 2019.

5.3. Across-track creep influence extent

Spatial influence extension of a creep can be estimated with a line-of-sight cumulative displacement time series. To investigate further I've taken 7 pairs of profiles from either side of the NAF. These pairs are starting from 500 m far from the fault on each side, ending at 3500 m, meaning a profile pair for every 500 meters. I've calculated the differences between each of these pairs. By comparing differences, it should be possible to find extension of creep influence in temporal scale. Swaths are again taken from 3 different values from either side of the fault centered at mentioned distances. I've selected profile (b) for the analysis on this section. Figure 5.6 shows temporal evolution of different swaths in 500 m, 1500 m, 3000 m of spatial extensions. The rest of the 500 m steps will be shown in a 2D plot.

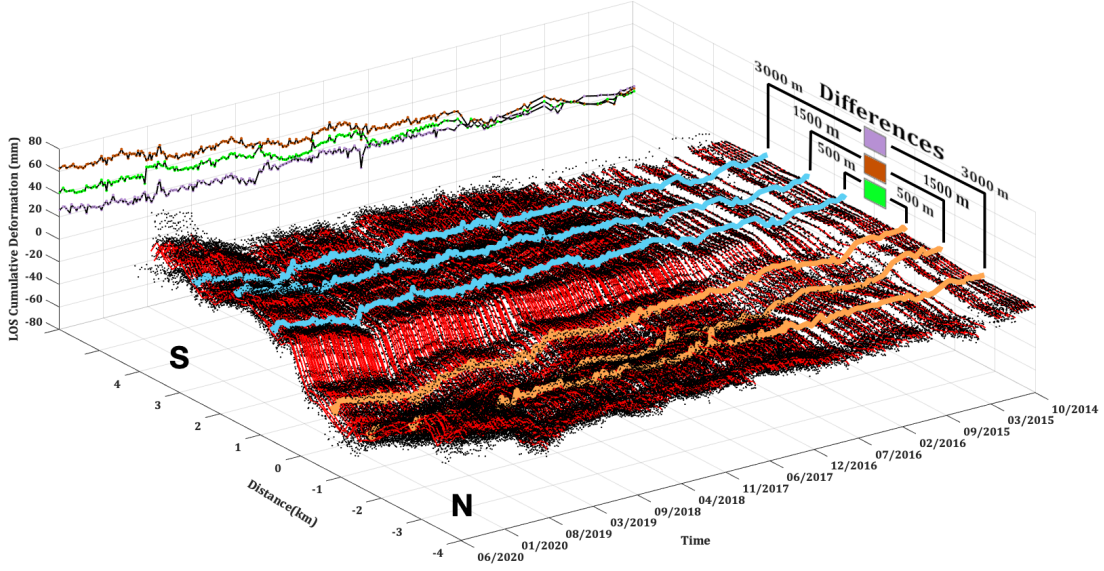


Figure 5.6: Swath pairs located at ~ 500 , ~ 1500 and ~ 3000 m either side from the fault. Green line shows the difference between swaths taken from 500 m apart from the fault (~ 1000 m apart from each other). Brown shows ~ 1500 m and purple shows ~ 3000 m.

It seems like the swath pair taken from 1500 m from the fault is exposing the maximum difference. If we assume the width of the main creeping area to be ~ 600 m (around “0” on Figure 5.6) green line which is closest to main creeping section shows the midmost deformation. And the swath pair that is furthest away from the fault, purple line, displays the minimum difference of the three. Figure 5.7 shows the temporal evolution of differences between 500 m swath steps taken from a ~ 300 m centered values. After setting up the swaths with ~ 500 m steps, I've fit the data using a curve fitting tool ([21] D'Errico, 2022). Linear fit has been done with a temporal separation of 6 months. The results indicate 3 diverse deformation groups. The maximum deformation happened at the middle-distance group from the fault, on swaths with 1000 and 1500 m distances. These are at ~ 10 mm/yr in LOS deformation rate. The second group consists of swaths with 500 m and 2000 m distances. These are showing average deformation, spatially these are forming both sides (North + South) of maximum deforming area. The rate of LOS deformation in this group is ~ 7 mm/yr. The third and least deforming group are swaths with distances of 2500, 3000 and 3500 m. These are expected to be showing least deformation since they are the farthest. The rate of their LOS displacement is ~ 4.5 mm/yr. My results show influence of tectonic creep is decreasing significantly with increasing perpendicular distance from the NAF. Especially between 2000 m and 2500 m, tectonic influence almost gets lost.

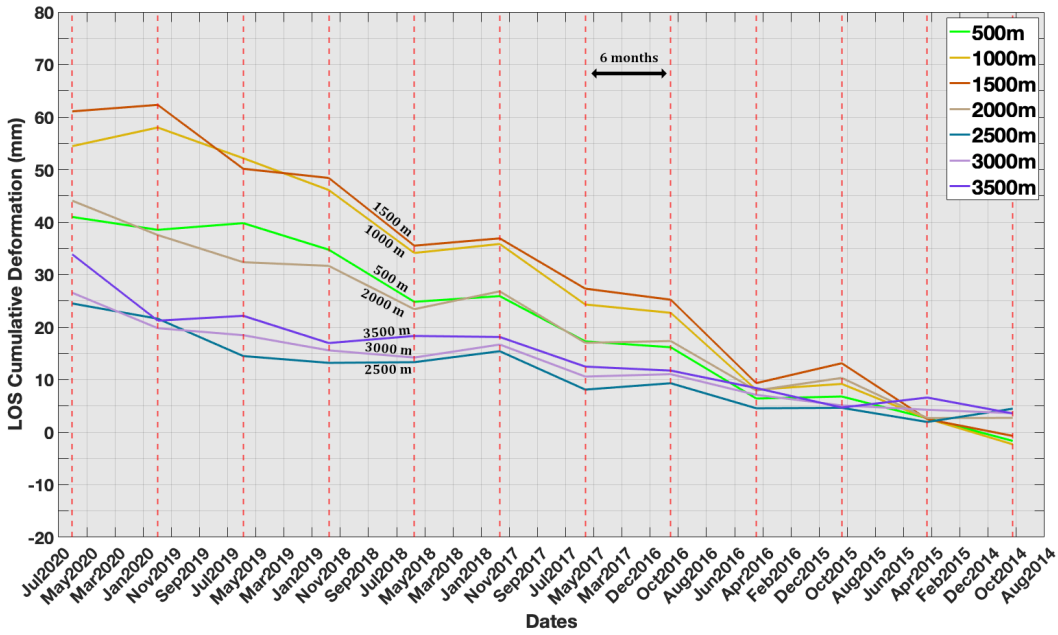


Figure 5.7: Temporal evolution of differences of swath pairs taken from every 500 m step distances from either side of North Anatolian Fault.

Note that third group start its journey back in 2014 with 5 mm LOS deformation advance. Also starting with April 2016 and May 2018, two group, highest deforming and midmost deforming lines start to increase in displacement. On the other hand, the farthest group is not deforming in those dates. Starting November 2019 there is a huge increase in displacement for the farthest group. This movement has more possibility to be a noise than a tectonic signal.

5.4. Episodic slip-burst on NAF

A slip burst of ~ 15 mm identified by [33] Rousset et al., 2016 with a time-series of 10 months, ending in March 2014 in a profile with same length, location, swath width with profile (b). I further proceed and extend the time series by ~ 6 more years starting from October 2014 until June 2020 to detect if more than one slip burst happened in the same area in the last ~ 6 years and if yes is there a pattern in temporal scale, like an episodic occurrence. I've used the difference between two swath pairs taken either side of the NAF from another ~ 300 m centered swaths, shown as a “green” line. There seems to be some relatively big jumps in the time series, especially on July 2016, 2017, and 2018 (Figure 4.12). I mostly eliminated signals before April 2016 and after April 2019. Before April 2016 the temporal resolution is relatively low since Sentinel-1B wasn't operating. After April 2019 there seems to be a major source of error that was affecting whole

raster. So, my temporal scale of focus is between April 2016 and April 2019. Different options for further analysis have been considered, including multi-month separated linear fit to data. 3, 6 and 12 months separated linear fit has been applied to the swath pair with ~ 250 m distance from the fault. 3 months separation with linear fit was the best option of the three. It's a good compromise between noise removal and tectonic signal. Figure 5.8 displays slip-burst candidates with their corresponding slope and LOS displacement rate values.

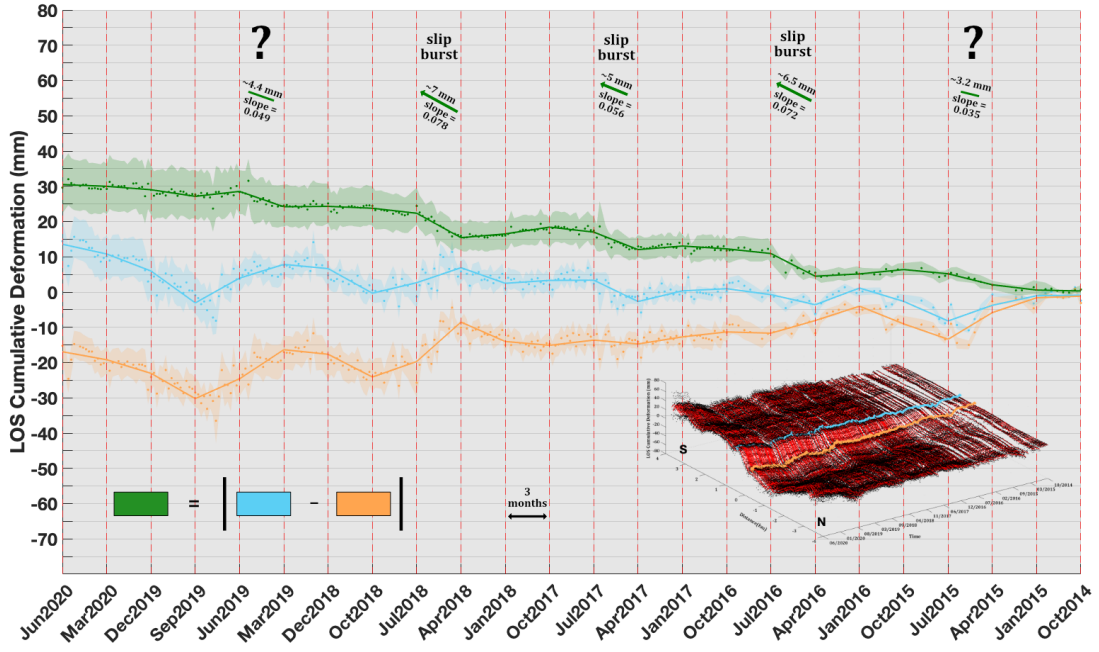


Figure 5.8: Linear fit in-between every 3 months for the swath pair with ~ 250 m distance from the fault for profile (b). 5 candidates for slip-bursts shown in the top side.

Starting from the beginning of time-series, in October 2014, difference between orange and blue lines (green line) does have a pattern of yearlong steps. Every creep-burst candidate accompanies with these steps. After temporal linear fitting of 3 months to the data, there are 5 clear parts with highest slopes. Two of them eliminated since they are showing the lowest slopes and lowest LOS displacement rates (first and last in time), and because of temporal and noise issues. Overall, 3 of slip-burst candidates are promising; June 2016, June 2017, June 2018. These are showing LOS displacement rate of ~ 6.5 mm, ~ 5 mm, ~ 7 mm in the same order. Furthermore, I've also linear fit the data horizontally. This way the difference between LOS cumulative displacement of each horizontal line would give creep-burst rate. Figure 5.9 shows duration of creep-burst candidates.

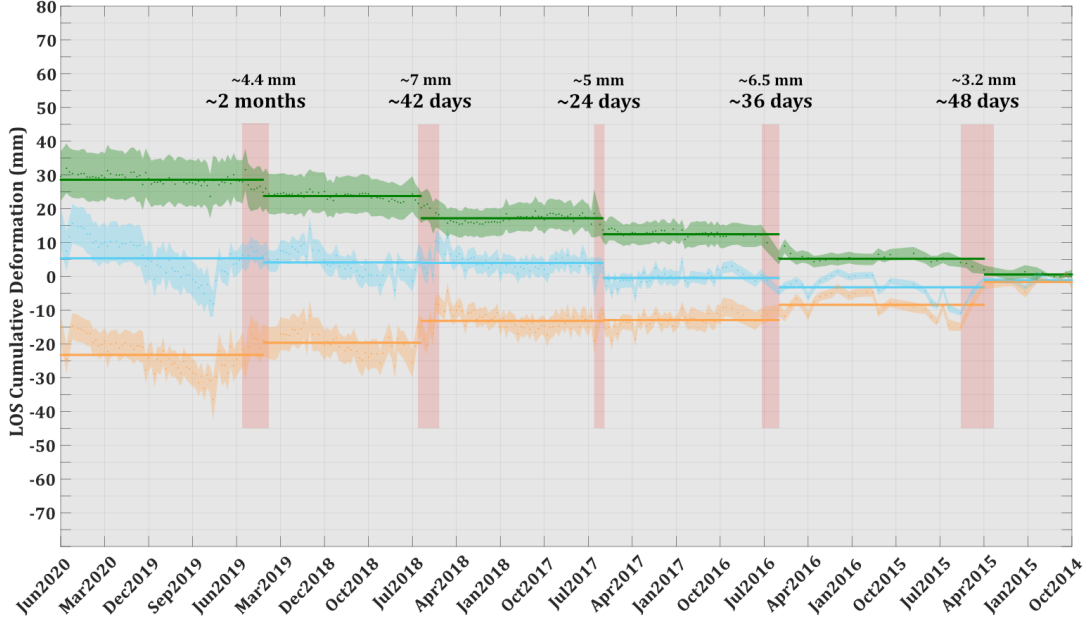


Figure 5.9: Horizontal fit for the time-series, separated with most abrupt signal changes. Red panel behind the lines show the duration of events.

Finally, I've applied a horizontal fit to time-series. This time I've used a method ([24] Killick et al., 2012) for detecting sudden change points which in our case corresponds to candidate creep-bursts. After detecting sudden change points, a horizontal linear fit has been applied to the time-series (Figure 5.9). A step pattern on all lines could be seen with red panels showing the duration of events. But there seems to be no correlation between LOS displacement rate and duration. There is a temporal correlation of jumps, which ~ 1 year in-between. Finally, according to my results after multiple fit methods applied to the data, 3 creep-burst events seem to have happened in June 2016, 2017, and 2018.

6. Conclusion

Using a high spatial and high temporal resolution Sentinel-1 InSAR dataset I've detected 3 concrete slip-burst events happened back-to-back in June 2016, June 2017, and June 2018 on Ismetpasa Segment of the North Anatolian Fault (NAF) in Turkey. Duration and LOS displacement rates for these events were ranging from 24 days to 42 days and ~5 to ~7 mm. This finding confirms a slip-burst found in 2014 August in the same area, by finding multiple another events. Furthermore, this study outspreads it to multiple events happening ~every year in this specific portion of the fault. I've also found out the creep-burst influence across-track. I've found the most slip-burst affected area to be in ~1500 m far from the fault, and influence steeply decrease after ~2250 m. In addition, with a high resolution InSAR enhanced strain map of Anatolia, I've detected multiple potential to be creeping areas on the NAF and in Turkey and potentially some previously unrecognized active faults.

A. Appendix

A.1. Noisy date pairs from all 3 profiles

After careful visual checking I've "changed" 2 pairs from profile (a), 3 pairs from profile (b) and 5 pairs (c) with closest date pair to them, resulted same date pair back-to-back. I've found that "changing" is a better solution than all together deleting the pair since closest pair to inconsistent pair supply an already interpolated image and better temporary consistency. Date pair means each set of black scatters. Figure A.1 shows changed data pairs with red points. Notice that all three profiles have 2 same date pairs changed, which is showing those pairs were consisted of mostly noisy signals. I've only changed those with high inconsistency and showing sudden anomalies. There are also some other pairs with sudden changes most distinct in profile (a), around 07/2017. But the pairs increasing and decreasing as it reaches to highest deformation so I've decided not to change it since it might have a concrete signal. So, when there is a high precision but low accuracy, I didn't change pairs. But when there is low precision accompanied by a low accuracy, like below figure's red pairs, they need to get removed.

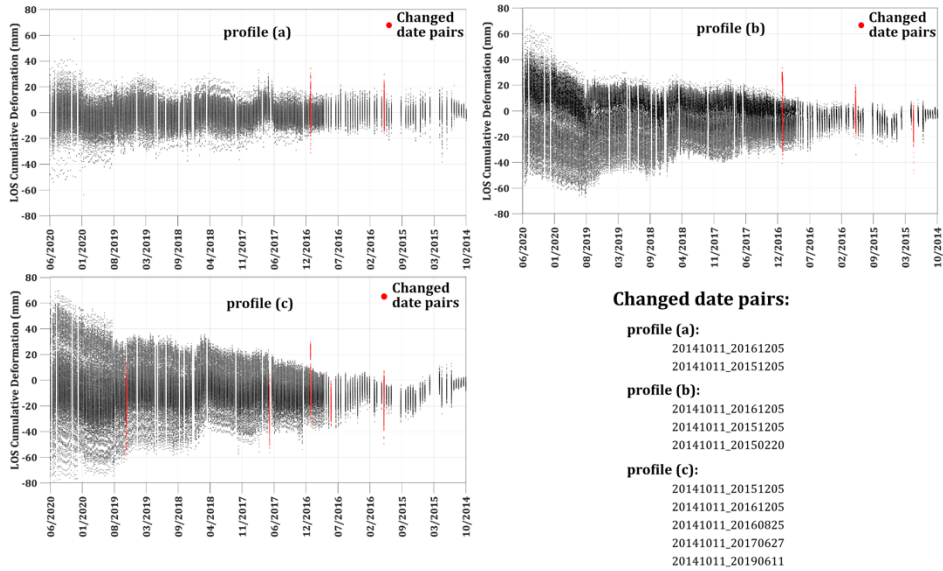


Figure A.1: A side view of 3D scatter time-series. Changed data pairs from profiles are shown with red scatters.

A.2. Automation of date pair creation

Below shell script is automated way of creating data pairs. The steps are further elaborated in Figure 4.5 and section 4.2.

```
#read reference and time-series date
read -p "Enter both dates: " FIRST SECOND

#creates .cum cumulative displacement float32 file using cum.h5 file
LiCSBAS_cum2flt.py -d ${SECOND} -m ${FIRST} -i TS_GEOCml1GACOSclip/TS_GEOCml1GACOSclip/cum_filt.h5 --ref_geo
32.444/32.474/40.923/40.937 --mask TS_GEOCml1GACOSclip/TS_GEOCml1GACOSclip/results/mask

#creates GeoTIFF file from cumulative displacement float32 file
LiCSBAS_flt2geotiff.py -i ${FIRST}_${SECOND}.cum -p TS_GEOCml1GACOSclip/TS_GEOCml1GACOSclip/info/EQA.dem_par

#convert GeoTIFF file to GMT grid file #-I is pixel size
gdal_translate -of netCDF ${FIRST}_${SECOND}.cum.geo.tif test.grd
GMT grd2xyz test.grd -s > trash.xyz
GMT xyz2grd trash.xyz -I.0.00099999210000007923/.000999999210000016596 -Rtest.grd -Gtest1.grd -Az

#rename test1.grd
mv test1.grd ${FIRST}_${SECOND}.cum.grd

#delete unnecessary files
rm -rf gmt.history ${FIRST}_${SECOND}.cum test.grd trash.xyz

#check if both files produced, if not display ERROR
[ -f ${FIRST}_${SECOND}.cum.grd -a -f ${FIRST}_${SECOND}.cum.geo.tif ] && echo both files OK || echo ERROR
```

It's possible to create date pairs with a list of dates supplied with below Python code.

```
import subprocess
import time

with open('dates_all.txt') as dates:
    for i in dates:
        print(i)
        output_string = subprocess.check_output(["sh","./cum_geotiff_and_grd.sh"],input=i,text=True)
        time.sleep(10)
```

A.3. Used dates

These dates are all the images used for the study area. Note that some of them are changed for certain profiles, more on appendix A.1.

20141011 20141023	20141011 20161111	20141011 20171001	20141011 20180902	20141011 20190804
20141011 20141104	20141011 20161117	20141011 20171007	20141011 20180908	20141011 20190810
20141011 20141116	20141011 20161123	20141011 20171013	20141011 20180914	20141011 20190816
20141011 20141128	20141011 20161129	20141011 20171019	20141011 20180926	20141011 20190822
20141011 20141210	20141011 20161205	20141011 20171025	20141011 20181002	20141011 20190828
20141011 20141222	20141011 20161211	20141011 20171031	20141011 20181008	20141011 20190903
20141011 20150103	20141011 20161217	20141011 20171106	20141011 20181014	20141011 20190909
20141011 20150127	20141011 20161223	20141011 20171112	20141011 20181020	20141011 20190915
20141011 20150220	20141011 20161229	20141011 20171118	20141011 20181026	20141011 20190921
20141011 20150304	20141011 20170104	20141011 20171124	20141011 20181101	20141011 20190927
20141011 20150421	20141011 20170116	20141011 20171130	20141011 20181107	20141011 20191003
20141011 20150515	20141011 20170122	20141011 20171206	20141011 20181113	20141011 20191009
20141011 20150527	20141011 20170128	20141011 20171218	20141011 20181119	20141011 20191015
20141011 20150608	20141011 20170203	20141011 20171224	20141011 20181201	20141011 20191021
20141011 20150702	20141011 20170209	20141011 20171230	20141011 20181207	20141011 20191027
20141011 20150714	20141011 20170215	20141011 20180105	20141011 20181213	20141011 20191102
20141011 20150726	20141011 20170221	20141011 20180111	20141011 20181219	20141011 20191108
20141011 20150807	20141011 20170227	20141011 20180117	20141011 20181225	20141011 20191114
20141011 20150819	20141011 20170305	20141011 20180123	20141011 20181231	20141011 20191120
20141011 20150912	20141011 20170311	20141011 20180129	20141011 20190112	20141011 20191126
20141011 20151030	20141011 20170317	20141011 20180204	20141011 20190124	20141011 20191202
20141011 20151111	20141011 20170323	20141011 20180210	20141011 20190130	20141011 20191208
20141011 20151123	20141011 20170329	20141011 20180216	20141011 20190205	20141011 20191214
20141011 20151205	20141011 20170404	20141011 20180222	20141011 20190211	20141011 20191220
20141011 20151217	20141011 20170410	20141011 20180228	20141011 20190217	20141011 20191226
20141011 20160110	20141011 20170416	20141011 20180306	20141011 20190223	20141011 20200101
20141011 20160122	20141011 20170422	20141011 20180312	20141011 20190301	20141011 20200107
20141011 20160215	20141011 20170428	20141011 20180318	20141011 20190307	20141011 20200113
20141011 20160227	20141011 20170504	20141011 20180324	20141011 20190313	20141011 20200119
20141011 20160310	20141011 20170510	20141011 20180330	20141011 20190319	20141011 20200125
20141011 20160322	20141011 20170516	20141011 20180405	20141011 20190325	20141011 20200131
20141011 20160403	20141011 20170522	20141011 20180411	20141011 20190331	20141011 20200212
20141011 20160415	20141011 20170528	20141011 20180417	20141011 20190406	20141011 20200218
20141011 20160427	20141011 20170603	20141011 20180423	20141011 20190412	20141011 20200224
20141011 20160509	20141011 20170609	20141011 20180429	20141011 20190424	20141011 20200301
20141011 20160521	20141011 20170615	20141011 20180511	20141011 20190430	20141011 20200313
20141011 20160602	20141011 20170627	20141011 20180517	20141011 20190506	20141011 20200319
20141011 20160614	20141011 20170703	20141011 20180523	20141011 20190512	20141011 20200325
20141011 20160708	20141011 20170709	20141011 20180529	20141011 20190518	20141011 20200331
20141011 20160720	20141011 20170715	20141011 20180604	20141011 20190524	20141011 20200406
20141011 20160801	20141011 20170721	20141011 20180610	20141011 20190530	20141011 20200412
20141011 20160825	20141011 20170727	20141011 20180616	20141011 20190605	20141011 20200418
20141011 20160906	20141011 20170808	20141011 20180622	20141011 20190611	20141011 20200424
20141011 20160918	20141011 20170814	20141011 20180628	20141011 20190617	20141011 20200430
20141011 20160930	20141011 20170820	20141011 20180704	20141011 20190623	20141011 20200506
20141011 20161006	20141011 20170826	20141011 20180722	20141011 20190629	20141011 20200512
20141011 20161012	20141011 20170901	20141011 20180728	20141011 20190705	20141011 20200518
20141011 20161018	20141011 20170907	20141011 20180803	20141011 20190711	20141011 20200530
20141011 20161024	20141011 20170913	20141011 20180809	20141011 20190717	20141011 20200605
20141011 20161030	20141011 20170919	20141011 20180815	20141011 20190723	20141011 20200611
20141011 20161105	20141011 20170925	20141011 20180821	20141011 20190729	20141011 20200623

Bibliography

- [1] Ambraseys, N.N., 1970. Some characteristic features of the Anatolian fault zone. *Tectonophysics*, 9(2-3), pp.143-165.
- [2] B.Ü. Kandilli Rasathanesi ve Dae. Bölgesel Deprem-Tsunami İzleme ve Değerlendirme Merkezi, 14 Eylül 2019 Çerkeş-Çankırı Depremleri, Basın Bülteni, http://koeri.boun.edu.tr/sismo/2/wp-content/uploads/2019/09/14_Eylul_2019_CANKIRI_Depremleri.pdf
- [3] Barka, A., 1996. Slip distribution along the North Anatolian fault associated with the large earthquakes of the period 1939 to 1967. *Bulletin of the Seismological Society of America*, 86(5), pp.1238-1254.
- [4] Barka, A., 1999. The 17 august 1999 Izmit earthquake. *Science*, 285(5435), pp.1858-1859.
- [5] Bilham, R., Ozener, H., Mencin, D., Dogru, A., Ergintav, S., Cakir, Z., Aytun, A., Aktug, B., Yilmaz, O., Johnson, W. and Mattioli, G., 2016. Surface creep on the North Anatolian fault at Ismetpasa, Turkey, 1944–2016. *Journal of Geophysical Research: Solid Earth*, 121(10), pp.7409-7431.
- [6] Bohnhoff, M., Bulut, F., Dresen, G., Malin, P.E., Eken, T. and Aktar, M., 2013. An earthquake gap south of Istanbul. *Nature communications*, 4(1), pp.1-6.
- [7] Bohnhoff, M., Wollin, C., Domigall, D., Küperkoch, L., Martínez-Garzón, P., Kwiatek, G., Dresen, G. and Malin, P.E., 2017. Repeating Marmara Sea earthquakes: indication for fault creep. *Geophysical Journal International*, 210(1), pp.332-339.
- [8] Bozkurt, E., 2001. Neotectonics of Turkey—a synthesis. *Geodinamica acta*, 14(1-3), pp.3-30.
- [9] Bürgmann, R., Schmidt, D., Nadeau, R.M., d'Alessio, M., Fielding, E., Manaker, D., McEvilly, T.V. and Murray, M.H., 2000. Earthquake potential along the northern Hayward fault, California. *Science*, 289(5482), pp.1178-1182.
- [10] Cakir, Z., Akoglu, A.M., Belabbes, S., Ergintav, S. and Meghraoui, M., 2005. Creeping along the Ismetpasa section of the North Anatolian fault (Western Turkey): Rate and extent from InSAR. *Earth and Planetary Science Letters*, 238(1-2), pp.225-234.
- [11] Cakir, Z., Ergintav, S., Özener, H., Dogan, U., Akoglu, A.M., Meghraoui, M. and Reilinger, R., 2012. Onset of aseismic creep on major strike-slip faults. *Geology*, 40(12), pp.1115-1118.
- [12] Cetin, E., Cakir, Z., Meghraoui, M., Ergintav, S. and Akoglu, A.M., 2014. Extent and distribution of aseismic slip on the Ismetpaşa segment of the North Anatolian Fault (Turkey) from Persistent Scatterer InSAR. *Geochemistry, Geophysics, Geosystems*, 15(7), pp.2883-2894.
- [13] COMET-LiCS product details. <https://comet.nerc.ac.uk/comet-lics-portal-product-details/>
- [14] Dewey, J.W., 1976. Seismicity of northern Anatolia. *Bulletin of the Seismological Society of America*, 66(3), pp.843-868.

- [15]Earth Surface Deformation and Radar Satellite Interferometry (InSAR) Class – Uni-Potsdam – Coregistration and Interferogram Formation Slide, Hannes Vasyura-Bathke, Sabrina Metzger.
- [16]Emery, B. and Camps, A., 2017. Introduction to satellite remote sensing: atmosphere, ocean, land, and cryosphere applications. Elsevier.
- [17]Emre, Ö., Duman, T.Y., Özalp, S., Saroğlu, F., Olgun, Ş., Elmacı, H. and Çan, T., 2018. Active fault database of Turkey. *Bulletin of Earthquake Engineering*, 16(8), pp.3229-3275.
- [18]Farr, T.G., Rosen, P.A., Caro, E., Crippen, R., Duren, R., Hensley, S., Kobrick, M., Paller, M., Rodriguez, E., Roth, L. and Seal, D., 2007. The shuttle radar topography mission. *Reviews of geophysics*, 45(2).
- [19]Hooper, A., Zebker, H., Segall, P. and Kampes, B., 2004. A new method for measuring deformation on volcanoes and other natural terrains using InSAR persistent scatterers. *Geophysical research letters*, 31(23).
- [20]Hussain, E., 2016. Mapping and modelling the spatial variation in strain accumulation along the North Anatolian Fault (Doctoral dissertation, University of Leeds).
- [21]John D'Errico (2022). SLM - Shape Language Modeling (<https://www.mathworks.com/matlabcentral/fileexchange/24443-slm-shape-language-modeling>), MATLAB Central File Exchange. Retrieved February 22, 2022.
- [22]Jolivet, R. and Frank, W.B., 2020. The transient and intermittent nature of slow slip. *AGU Advances*, 1(1), p.e2019AV000126.
- [23]Ketin, I., 1948. Über die tektonisch-mechanischen Folgerungen aus den grossen anatolischen Erdbeben des letzten Dezenniums. *Geologische Rundschau*, 36(1), pp.77-83.
- [24]Killick, R., Fearnhead, P. and Eckley, I.A., 2012. Optimal detection of changepoints with a linear computational cost. *Journal of the American Statistical Association*, 107(500), pp.1590-1598.
- [25]Kreemer, C., Blewitt, G. and Klein, E.C., 2014. A geodetic plate motion and Global Strain Rate Model. *Geochemistry, Geophysics, Geosystems*, 15(10), pp.3849-3889.
- [26]Lazecký, M., Spaans, K., González, P.J., Maghsoudi, Y., Morishita, Y., Albino, F., Elliott, J., Greenall, N., Hatton, E., Hooper, A. and Juncu, D., 2020. LiCSAR: An automatic InSAR tool for measuring and monitoring tectonic and volcanic activity. *Remote Sensing*, 12(15), p.2430.
- [27]López-Quiroz, P., Doin, M.P., Tupin, F., Briole, P. and Nicolas, J.M., 2009. Time series analysis of Mexico City subsidence constrained by radar interferometry. *Journal of Applied Geophysics*, 69(1), pp.1-15.
- [28]Mohr, J.J., Reeh, N. and Madsen, S.N., 1998. Three-dimensional glacial flow and surface elevation measured with radar interferometry. *Nature*, 391(6664), pp.273-276.
- [29]Morishita, Y., Lazecký, M., Wright, T.J., Weiss, J.R., Elliott, J.R. and Hooper, A., 2020. LiCSBAS: an open-source InSAR time series analysis package integrated with the LiCSAR automated Sentinel-1 InSAR processor. *Remote Sensing*, 12(3), p.424.
- [30]Osmanoğlu, B., Sunar, F., Wdowinski, S. and Cabral-Cano, E., 2016. Time series analysis of InSAR data: Methods and trends. *ISPRS Journal of Photogrammetry and Remote Sensing*, 115, pp.90-102.

- [31] Ou, Q., Daout, S., Weiss, J., Shen, L., Lazecky, M., Wright T. J., and Parsons, B. E. 2022. Large-scale Interseismic Strain Mapping of the NE Tibetan Plateau from Sentinel-1 Interferometry, preprint, <https://doi.org/10.1002/essoar.10510544.1>, ESSOAR.
- [32] Propagation of errors, LSU website.
<https://www.geol.lsu.edu/jlorenzo/geophysics/uncertainties/Uncertaintiespart2.html>
- [33] Reilinger, R., McClusky, S., Vernant, P., Lawrence, S., Ergintav, S., Cakmak, R., Ozener, H., Kadirov, F., Guliev, I., Stepanyan, R. and Nadariya, M., 2006. GPS constraints on continental deformation in the Africa-Arabia-Eurasia continental collision zone and implications for the dynamics of plate interactions. *Journal of Geophysical Research: Solid Earth*, 111(B5).
- [34] Rousset, B., Jolivet, R., Simons, M., Lasserre, C., Riel, B., Milillo, P., Çakir, Z. and Renard, F., 2016. An aseismic slip transient on the North Anatolian Fault. *Geophysical Research Letters*, 43(7), pp.3254-3262.
- [35] Şengör, A.M.C., Tüysüz, O., Imren, C., Sakınç, M., Eyidoğan, H., Görür, N., Le Pichon, X. and Rangin, C., 2005. The North Anatolian fault: A new look. *Annu. Rev. Earth Planet. Sci.*, 33, pp.37-112.
- [36] Sentinel-1 Mission overview, Copernicus Website.
<https://sentinels.copernicus.eu/web/sentinel/missions/sentinel-1>
- [37] Stein, R.S., Barka, A.A. and Dieterich, J.H., 1997. Progressive failure on the North Anatolian fault since 1939 by earthquake stress triggering. *Geophysical Journal International*, 128(3), pp.594-604.
- [38] Tung, H. and Hu, J.C., 2012. Assessments of serious anthropogenic land subsidence in Yunlin County of central Taiwan from 1996 to 1999 by Persistent Scatterers InSAR. *Tectonophysics*, 578, pp.126-135.
- [39] Weiss, J.R., Walters, R.J., Morishita, Y., Wright, T.J., Lazecky, M., Wang, H., Hussain, E., Hooper, A.J., Elliott, J.R., Rollins, C. and Yu, C., 2020. High-resolution surface velocities and strain for Anatolia from Sentinel-1 InSAR and GNSS data. *Geophysical Research Letters*, 47(17), p.e2020GL087376.
- [40] Widening Envisat's InSAR view, ESA website. https://esa.int/Applications/Observing-the_Earth/Widening_Envisat_s_InSAR_view
- [41] Woodhouse, I.H., 2017. Introduction to microwave remote sensing. CRC press.
- [42] Yamamoto, R., Kido, M., Ohta, Y., Takahashi, N., Yamamoto, Y., Pinar, A., Kalafat, D., Özener, H. and Kaneda, Y., 2019. Seafloor geodesy revealed partial creep of the North Anatolian Fault submerged in the Sea of Marmara. *Geophysical Research Letters*, 46(3), pp.1268-1275.
- [43] Yu, C., Li, Z. and Penna, N.T., 2018. Interferometric synthetic aperture radar atmospheric correction using a GPS-based iterative tropospheric decomposition model. *Remote Sensing of Environment*, 204, pp.109-121.